

Design of iron oxide nanoparticles as theranostic nanoplatforms for cancer treatment

Thomas Gevart^a, Barbara Freis^{a,b}, Thomas Vangijzegem^a, Maria Los Angeles Ramirez^b, Dimitri Stanicki^a, Sylvie Begin^b, Sophie Laurent^a.

^a) Department of General, Organic and Biomedical Chemistry, NMR and Molecular Imaging Laboratory, UMONS, 19 Avenue Maistriau, 7000 Mons, Belgium

^b) Université de Strasbourg, CNRS, Institut de Physique et Chimie des Matériaux, UMR CNRS-UdS 7504, 23 Rue du Loess, BP 43, 67034 Strasbourg, France

Abstract:

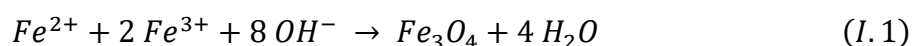
This chapter describes the structure and magnetic properties of iron oxide nanoparticles (IONPs), which are currently being developed for biomedical applications, especially in the case of cancer treatment. Cancer is a major public health issue worldwide, with increasing incidence and mortality rates. According to the Global Cancer Observatory (GLOBOCAN), it is the second leading cause of death globally, after ischemic heart disease; responsible for an estimated 9.6 million deaths in 2018. Early diagnosis is essential for effective treatment and management. Patients with early-stage cancers have a better chance of survival and may require less aggressive treatments, leading to a better quality of life. However, detecting cancer at an early stage is challenging due to the lack of sensitive and specific diagnostic tools. Furthermore, conventional treatments such as chemotherapy and radiation therapy are efficient but show limitations due to the non-specific targeting of cancer cells and potential toxicity to healthy tissues. Therefore, there is a need for the development of both novel diagnostic methods that can accurately detect cancer at an early stage as well as novel therapeutic strategies that are more effective and less toxic. Iron oxide nanoparticles (IONPs) represent an interesting solution, offering implementation of a theranostic approach. Thanks to their magnetic properties, the particles act as contrast agents for magnetic resonance imaging (MRI) but also as therapeutic agents for magnetic hyperthermia (MH) or as drug delivery systems. Here the different ways to synthesize nanoparticles are quickly described, the thermal decomposition method is emphasized as it allows a fine control of the nanoparticles size distribution. Then biological applications of nanoplatforms designed for theranostics will serve as examples to emphasize the interest of these materials.

Iron oxide nanoparticles for MRI

Synthesis of IONPs

Current challenges in the synthesis of IONPs are to obtain controlled nanoparticles in terms of composition, size, shape, and crystallinity by avoiding undesired reactions and the use of too many reactants¹. The specifications on the design of IONPs for combining dual treatment via magnetic hyperthermia lead to investigate the effect of the size and shape of IONPs. A synthesis method allowing easy modulation of the size and shape of IONPs and leading to a narrow size distribution and high colloidal stability is needed.

90 % of superparamagnetic IONPs are synthesized by chemical methods according to Ali *et al.*², even if physical and biological methods keep showing great interest^{2,3}. Among the chemical methods, coprecipitation, a method developed by Massart *et al.* is the most used one⁴. Iron (II) and iron (III) salts are dissolved in an aqueous solution and are precipitated after the addition of a base through this global reaction:



The main advantage of this method is the production of IONPs with a high yield directly in water with an easy-to-process and cheap method. However, if no ligand is added during the synthesis, NPs tend to form aggregates, as they are 'naked'. Nonetheless, the addition of ligand during the process can disrupt the formation of NPs and lead to NPs with no good control of size or shape⁵.

Thus, through the years, other methods have been developed to improve the control of size, shape, and colloidal stability of the synthesized nanoparticles. Among them, microemulsion, polyol synthesis, hydrothermal, or microwave-assisted synthesis can be cited¹. Another growing method since the early 2000s is thermal decomposition (TD). Most reported methods are summarized Table 1 with their ability to control the size and shape of IONPs^{1,6}.

Table 1- Size and shape control of the most reported synthesis methods of iron oxide NPs (adapted from ¹).

Method	Process conditions (temperature, process time, handling)	Dispersity	Shape control	Yield
Co-precipitation	Low T°, minutes, complicated ++	Average	Bad (irregular sphere)	High
Microemulsion	Low T°, hours, complicated	± Narrow	Very good (cube-sphere)	Poor
Sol-gel	Low T°, hours, simple	± Narrow	Good (sphere)	Poor
Hydrothermal	High T°, hours, simple	± Narrow	Bad (irregular sphere)	High
Thermal decomposition	High T°, hours-days, complicated ++	Very narrow	Very good (cube-sphere)	High

The thermal decomposition synthesis method is generally designated as the most suitable one to obtain particles with controlled size and shape as well as colloidal stability. First introduced by Hyeon's and Sun's research groups^{7,8}, this method rapidly gathered interest among researchers because of its various advantages. Indeed, this method allows synthesizing IONPs with a high yield. The NPs are also coated *in situ* with a surfactant, thus do not agglomerate, and present high monodispersity in size. Moreover, the synthesis allows precise control of both particle size and shape, which can be tuned by changing synthesis parameters such as the nature of reactants, the nature of solvents, the heating rate or the reaction duration. However, the synthesis requires quite harsh conditions, as the mixture needs to be heated at a high temperature for several hours in a high boiling point organic solvent. The surfactants are generally hydrophobic and ligand exchange is necessary to make the NPs stable in water and physiological media for further biological applications.

Principles of the TD method

The TD method was at first used for the synthesis of quantum dots and semi-conductor nanocrystals in the late 1990s^{9,10}. An organometallic complex is brought to high temperature in a high boiling point organic solvent and in the presence of a surfactant to stabilize the formed NPs (Figure 1-A). The TD process leads to the decomposition of the precursor and the generation of monomers, which then trigger the formation of small nuclei. Then, depending on the reaction temperature and time, these nuclei will next grow into well-crystallized NPs stabilized by the surfactant coating (Figure 1-B). This method allows a good separation between the nucleation and growth steps, which is a prerequisite to control the size distribution. Indeed, it follows the LaMer and Dinegar theory of nucleation and growth of particles, introduced in 1950 to explain the formation of monodisperse hydrosols¹¹. This theory is based on three different steps depending on the concentration of monomers in solution and it is generally applied to the mechanism of NPs formation via TD¹².

Three major stages are thus proposed for the IONPs synthesis (Figure 1):

- i) iron-based monomer generation (monomers are reported to result from the precursor decomposition upon increasing temperature)¹³.
- ii) nucleation after which a critical nucleation concentration (C_{min}^{nu}) in monomer is reached.
- iii) growth of nuclei after which the monomer concentration falls below C_{min}^{nu} but stays above the saturation C_s . Therefore, nuclei are generated during a nucleation step that is followed by a homogeneous growth step without the creation of new nuclei¹³⁻¹⁵.

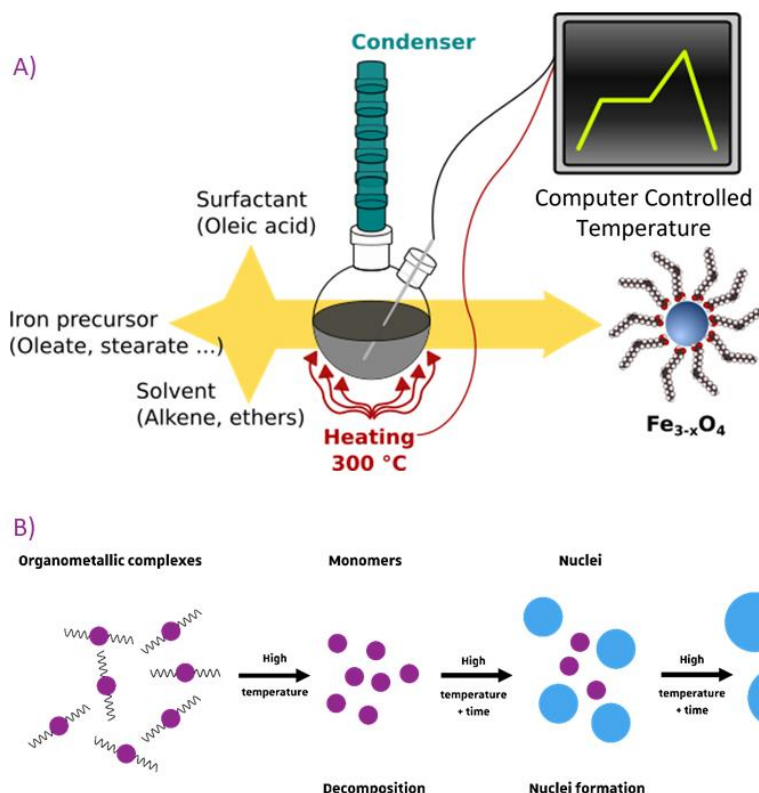


Figure 1 - A) Schematic representation of the thermal decomposition method and B) The three major steps of the TD synthesis.

LaMer theory can thus explain NPs synthesis with a narrow size distribution and the possibility to obtain different shapes using shape-driving ligands. Nevertheless, a continuous growth process from monomer has also been proposed^{16,17} and a recent study reported that instead of a homogeneous nucleation within the solvent, the nucleation occurs within vesicle-like “nanoreactors” which confine the reactants¹⁸. The nature of ligand and solvent used also have an impact on the stability of the precursor and its decomposition process¹⁴. The TD synthesis with its variety of experimental parameters such as temperature, reaction time, concentration and nature of precursors, surfactants and solvent offers great freedom in the design of NPs (e.g. to tune the size, morphology and composition).

IONPs synthesis by the TD method has been developed since the early 2000s^{7,8,19}. The most common iron precursors are $\text{Fe}(\text{acac})_n$ (acac = acetylacetonate)^{20–22} and iron oleate^{23–29} (unsaturated C18) but other precursors are also used such as iron stearate^{14,16,30–33} (saturated C18) or carbonyls $\text{Fe}(\text{CO})_x$ ^{34,35}. The boiling point of organic solvents must be quite high to decompose the precursor and is generally in the range 270 °C to 350 °C. For this reason, mainly alkenes and ethers are used^{36–38}. Finally, commonly used surfactants are fatty acids like oleic acid (OA) and sometimes mixtures of fatty acids³⁹. Their role is crucial as they stabilize the formed NPs and prevent them from aggregation by Van der Waals and dipolar interactions.

Two ways of performing the thermal decomposition of iron precursors are possible. The first one is the ‘hot injection’ method where the iron precursor is directly injected into the solvent and surfactant mixture, already heated at high temperature⁴⁰. The iron precursor will directly decompose. However, this quite abrupt method presents some issues for shape control and

it is not suited for scale-up⁴¹. The second one is the 'heating-up' method, where the precursor is solubilized with the surfactant in the organic solvent at ambient temperature and the mixture is heated up to the boiling temperature of the solvent. This method allows more control of the decomposition⁴².

By tuning various parameters of the TD method such as the nature of solvent, of precursors and of the surfactants, the amount and the number of surfactants, the concentration of reactants but also the reaction duration, IONPs with different sizes and shapes may be synthesized⁴³. The strength of this method comes from the observed separation between the nucleation stage and the growth stage. However, as the parameters influencing NPs size, shape and composition are completely linked and entangled together, it is still difficult to fully understand the process and to predict exactly how a parameter influences the final synthesized NPs.

To obtain nanoparticles with a diameter higher than 15 nm, the synthesis needs to ensure a longer growth step or to favor a low yield in nuclei during the nucleation step preserving monomers for the growth step. The main parameters reported to tune the size of IONPs are the nature of the solvent, the reaction temperature and the surfactant to iron precursor ratio^{14,37,44,45}. However, an impact of the solvent, precursor and reaction time have also been evidenced¹⁴.

❖ Reaction temperature tuned by the nature of solvents

The effect of the solvent is mostly related to its boiling point; the higher it is, the larger the NPs diameter should be. Indeed, a higher boiling point and a longer growth step should yield more monomers (as some iron precursors decompose on large temperature range). However, the nature of the solvent (*e.g.* its polarity) may also affect the NPs size by affecting the precursor's thermal stability and thus its decomposition¹⁴. Highly polar organic solvents would favor the decomposition of a large amount of precursor, inducing germination of small nuclei with less monomer available for the grain growth step: small-sized NPs are thus obtained.

Non-polar solvents such as alkenes do not interact with iron precursors and so the diameter increases in a quite linear way with the solvent boiling point. This confirms that the growth rate mainly depends on the reaction temperature. In that context, docosene is suitable to synthesize IONPs with a mean size around 20 nm. However, docosene is solid at ambient temperature (its melting temperature is at 62 °C) which makes the washing and purification steps difficult. Some groups prefer to work with an alkane solvent squalane, which is not solid at ambient temperature and presents a high boiling point of 470 °C^{43,46,47}. However, as its boiling point is so high, we cannot use it at the boiling point to avoid degradation of the alkyl chains of the reactants. Thus, the temperature has to be kept below the boiling point where it is less controlled. It was observed that depending on the effective reaction temperature, some variations in the composition from a spinel phase to core-shell NPs with a wüstite core occur⁴⁸. A low heating rate during the growth step was shown to be promising to ensure a spinel composition⁴⁸. The addition of a small amount of dibenzyl ether (DBE) with octadecene or squalane solvent would provide a more oxidative environment and allow IONPs with mean size higher than 15 nm and a spinel composition to be obtained^{47,49–52}.

❖ Influence of the molar ligand/precursor ratio

Numerous studies have been conducted on this parameter; the influence of the amount of ligand on the NPs size is quite complex^{14,45,53,54}, either an increase^{55,56} or the opposite trend⁵⁷ was observed. Bronstein *et al.*⁵⁴ observed an evolution with iron oleate and oleic acid in eicosane without proposing an explanation, while Salas *et al.*⁴⁵ reported an influence of oleic acid on nucleation and growth rates. Indeed, two competitive mechanisms may occur. First a higher stabilization of the iron complex, with the increased amount of oleic acid which thus decomposes at higher temperature. But also, a stronger stabilization of nuclei affecting the grain growth. Thus, this parameter appears more complex to tune to control the growth of IONPs.

❖ Reaction time

Another obvious parameter to increase the size of the NPs is the reaction time. Baaziz *et al.* made experiments on the established 10 nm protocol and concluded that an increase in reaction time leads to an increase of size from 10 nm up to 14/15 nm after 6 hours¹⁴. Adapting the reaction time with solvents with higher boiling point could be a way to reach sizes around 20 nm.

❖ Effect of the nature of precursors

Hufschmid *et al.*⁵⁸ also demonstrated that some precursors are more suited for IONPs synthesis of specific size ranges. Bronstein *et al.* evidenced an effect of washing and aging conditions of iron oleate⁵⁹ and alkyl chain length⁴⁴ on the IONPs size and shape. Recent research work has been conducted to improve the quality and stability of the iron oleate precursor (reported highly sensitive to minor variations in its synthesis due to its propensity to retain water, oleic acid, and other reaction by-products) by performing different washing or drying treatments. These treatments were found efficient to better stabilize the iron oleate precursor and obtain IONPs with larger sizes, up to 40 nm^{50,60,61}.

The investigation of the thermal decomposition of both iron stearate FeSt₂ and FeSt₃ precursors in standard synthesis conditions of 10 nm spherical NPs (dioctylether as solvent and oleic acid as surfactant) led to spherical NPs with a monocrystalline structure and a homogeneous Fe_{3-x}O₄ composition; only the size was slightly affected by the nature of iron stearate (about 9 nm with FeSt₃ and 10 nm with FeSt₂)³⁸. This was attributed to the fact that the decomposition kinetics of FeSt₂ at temperature below 298 °C was higher than that of FeSt₃, which decomposes in a larger temperature range up to 350 °C. When the TD experiments occur in solvent or mixture of solvents with higher boiling point to obtain IONPs with higher size, an impact of iron stearates was observed. Only with FeSt₃, IONPs with sizes higher than 15 nm were obtained. When FeSt₂ is used as a precursor, an increase of the size is observed, but it stays lower than 15 nm. Indeed, FeSt₂ decomposes mainly below 300 °C and only few precursors are available for the growth step by contrast with FeSt₃, which decomposes up to 350 °C and provides monomers during the growth step^{48,62}.

IONPs composition

At the nanoscale, oxidation phenomenon becomes much more important than at the bulk scale. Indeed, at the nanoscale, the iron (II) cations in magnetite $(\text{Fe}^{3+})_A[\text{Fe}^{2+}\text{Fe}^{3+}]_B\text{O}_4$ (where A represents the cations in the tetrahedral sites and B those in the octahedral sites) become highly sensitive to oxidation especially those located at the surface of the NP^{14,63–66}. This Fe^{2+} oxidation is very sensitive to the IONPs size and thus, a IONPs size dependent composition was observed in nanoparticles synthesized by coprecipitation^{64,67} and by thermal decomposition¹⁴. In the case of the thermal decomposition method, Baaziz *et al.*¹⁴ have shown that when NPs have a diameter smaller than 8 nm, the oxidation phenomenon of Fe(II) cation into Fe(III) cation is quite total. So, the NPs have a composition very close to that of the maghemite phase. For IONPs with a diameter higher than 12 nm, the oxidation of Fe(II) cations takes place mainly at their surface. Thus, the IONPs are composed of a magnetite core and an oxidized layer at the surface ($\text{Fe}_{3-x}\text{O}_4$) and the higher is the NP size, the higher is the size of the magnetite core. When the diameter is intermediate (this means above 8 nm but below 12 nm), the magnetite phase is partially oxidized without the appearance of a core-shell structure. Thus, the overall composition is described as being $\text{Fe}_{3-x}\text{O}_4$. Further Mössbauer spectrometry characterizations have shown the presence of oxidation defects, surface and volume spin canting as a function of NPs diameter⁶⁸.

Small NPs presented mainly a surface spin canting. NPs with larger sizes display different oxidized shell thickness, defects and surface spin canting. NPs with intermediate sizes display a surface and in particular a volume spin canting due to a disordered structure induced by a perturbed oxidation state in these NPs⁶⁹.

During the synthesis of IONPs larger than 15 nm^{38,43,70} or with different shapes such as the cubic form^{71–73}, the formation of core-shell structures with a wüstite core and a spinel shell ($\text{Fe}_{1-x}\text{O}@\text{Fe}_{3-x}\text{O}_4$) has often been reported. One main reason is that the nuclei formed during the TD process have a wüstite composition. To increase the size of IONPs, the synthesis is performed at higher temperature to favor the growth step and organic solvents with higher boiling point are used. These solvents are often non-polar solvents such as squalane or octadecene providing a reducing environment which is not favorable for oxygen diffusion.

For the standard synthesis of 10 nm IONPs, the final composition of IONPs corresponds to oxidized magnetite $\text{Fe}_{3-x}\text{O}_4$. This suggests that the oxidation of nuclei has occurred simultaneously with their growth and this is in agreement with the fact that the nucleation occurs at about 280 °C, a temperature which is very close to the boiling point of octylether (290 °C)^{18,33,38,74,75}. Octylether would not provide a reducing environment by contrast with alkene solvents and the heating time of 2 h at this boiling point should favor the oxidation of the wüstite nuclei. In fact, problems arise when trying to synthesize IONPs with sizes higher than 15 nm^{14,38}. Indeed, if the oxidation kinetics is too slow compared to the growth kinetics, which is an issue often appearing, core-shell structures are obtained (Figure 2). If an iron oxide spinel structure is identified, the IONPs often contain defects^{14,38,70,76}. It has often been reported that the oxidation of wüstite induces the presence of defects such as dislocations or antiphase boundaries observed as function of the IONPs size^{38,43,49–51,70,71,76,77}. Such defects

have a high impact on the magnetic properties of IONPs and thus on their magnetic hyperthermia performances^{78,79}.

The solvent nature, a too dense surfactant layer at the surface of nuclei, a high heating rate are among reported parameters hampering a good oxidation kinetics. More and more studies demonstrated that the addition of DBE is a good way to avoid the formation of core-shell IONPs^{47,49–52}. Indeed, the solvent's redox activity would be very important to control the valence state of iron. Thermolysis of aromatic ethers produces oxidizing species that stabilize the inverse spinel phase, while alkene hydrocarbons have reducing effects which can favor the formation of wüstite. Controlling this non-aqueous redox environment enables reproducible and scalable synthesis of nearly defect-free IONPs in the 10–30 nm range without the need for post-synthesis modification^{50–52,80,81}. This “non-aqueous redox phase-tuning” method is a very suitable method to avoid the formation of the wüstite phase during the nanoparticle growth process. Indeed, redox active species, coming from alkene solvents such as 1-octadecene and from ether solvents such as DBE, are generated during the high temperature synthesis stage. Specifically, DBE decomposition generates benzaldehyde, which possesses oxidative character⁵². On the contrary, the tendency of the 1-octadecene's vinyl group to oxidation produces a reductive effect.

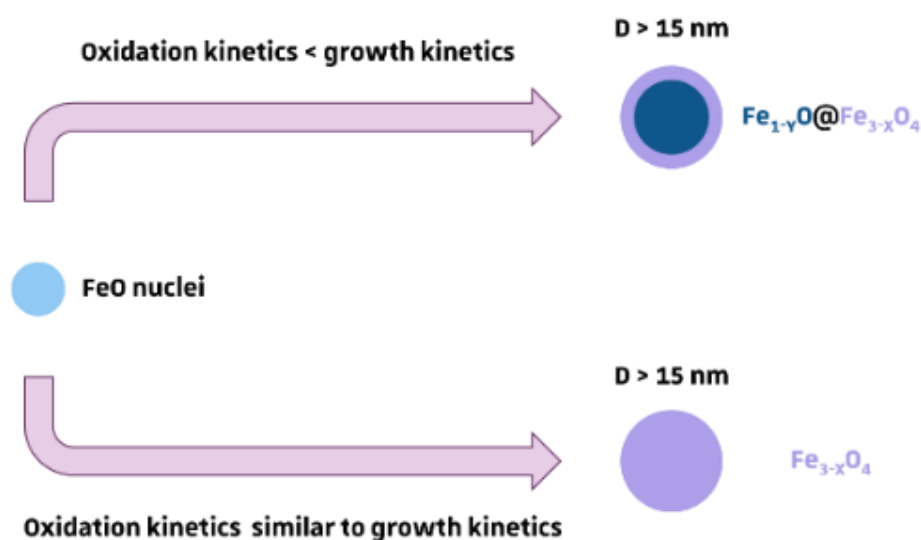


Figure 2 - Two possible compositions of big-sized IONPs (diameter > 15 nm) depending on the oxidation rate.

The competition between growth and oxidation depends greatly on the synthesis methods and the reactants present during synthesis. The oxidation of the wüstite core during synthesis can also lead to various amount of structural defect in a NP. Moreover, this core-shell structure and the presence of defects can greatly alter the magnetic properties.

Magnetic properties of IONPs

Magnetic properties of bulk magnetite and maghemite

Magnetic properties of bulk magnetite, maghemite and wüstite

Magnetic materials are described thanks to three main parameters: their magnetic moment μ corresponding to the tendency of their dipoles to align under an external magnetic field H , their magnetization M corresponding to the magnetic moment per volume, and their magnetic susceptibility χ corresponding to the propensity of the material to align its magnetization M to the external magnetic field H . The relation between magnetization and the external magnetic field is given by:

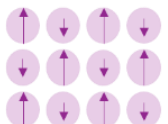
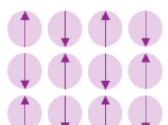
$$M = \chi H \quad (\text{I. 2})$$

From the magnetization can be extracted the maximum of magnetization called saturation magnetization which is an important criterion to distinguish magnetic materials.

The wüstite, magnetite, and maghemite phases present different types of magnetism. The wüstite phase presents antiferromagnetic properties⁸², which means that it has no magnetism without any field applied, and low magnetic properties when one is applied (Table 2). Maghemite and magnetite are both ferrimagnetic below their Curie temperature (858 K for magnetite⁸³ and 890 K for maghemite⁸⁴) and thus present a spontaneous magnetic spin organization with an anti-parallel alignment and without compensation of the moment (Table 2).

The magnetic ordering disappears above the Curie temperature for ferrimagnetic compounds. The thermal agitation is sufficient to suppress spontaneous magnetization, and the compound becomes paramagnetic. This means that there is no magnetic order anymore without any field applied.






Table 2 - Magnetic behavior of the wüstite, the maghemite and the magnetite phases at the bulk scale.

Types of magnetism	Susceptibility χ	Magnetic moment μ and atomic behavior	
Ferrimagnetism Fe₃O₄, γ-Fe₂O₃ phases	Large and positive, function of the applied field H	Anti-parallel aligned magnetic moments without compensation	
Antiferromagnetism FeO phase	Small and positive	Anti-parallel aligned magnetic moments with compensation	

Ferrimagnetism of the magnetite phase is due to the presence of both iron (II) and iron (III) in octahedral and tetrahedral sites as shown in Table 3. The magnetic moment of iron (III) in octahedral and tetrahedral sites can compensate. So, the magnetic moment of magnetite is determined by the moment of iron (II) in the octahedral site and is thus equal to 4 Bohr magneton (μ_B) which is a constant corresponding to the moment of an electron. The saturation magnetization of bulk magnetite is estimated to be 92 Am²/kg. For the maghemite

phase, there are only iron (III) cations that have a moment of $5 \mu_B$ in octahedral sites and tetrahedral sites. However, as vacancies also occupy octahedral sites, there are only $5/3$ of iron (III) in octahedral sites which gives an overall moment equal to $(\frac{5}{3} - 1) \times 5 \mu_B$ leading to a saturation magnetization of $74 \text{ Am}^2/\text{kg}$.

Table 3 - Magnetic structure, magnetic moment, and saturation magnetization of magnetite and maghemite.

Iron oxides	Cations	Octahedral sites	Tetrahedral sites	Magnetic moment	Magnetization saturation M_s (Am^2/kg)
Magnetite	Fe^{3+}	 $5 \mu_B$	 $-5 \mu_B$	Cancellation	92
	Fe^{2+}	 $4 \mu_B$		$4 \mu_B$	
Maghemite	Fe^{3+}	 $\frac{5}{3} \times 5 \mu_B$	 $-5 \mu_B$	$3.33 \mu_B$	74

At the bulk scale, ferrimagnetic materials present a magnetic structure made of domains called Weiss domains and separated by Bloch walls. This structure aims to diminish the internal energy of the material⁸². The magnetization is uniform within each domain but varies from one domain to another so that in the absence of an external magnetic field, there is no global magnetization.

When exposed to a magnetic field, the walls are moving so that domains with the same orientation as the applied field extend (Figure 3). Structural defects can slow down this effect, which implies a delay in the magnetic response of the material. After this first exposure to a magnetic field, the material is always magnetized and keeps a permanent magnetization.

This phenomenon is at the origin of the hysteresis loop observed on the magnetization curve with a remanent magnetization M_R , a saturation magnetization M_S and a coercive field H_C characteristic of the studied material.

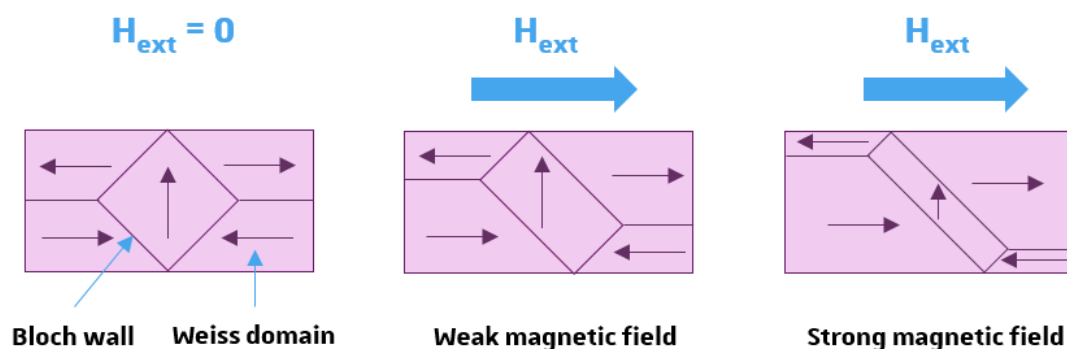


Figure 3 - Creation of Weiss domain to diminish internal energy and behavior under a magnetic field.

Anisotropy energy

The magnetization vector in a ferrimagnetic crystal is not isotropic, the direction of the spins with respect to the crystal lattice depends on the magnetocrystalline anisotropy. This anisotropy comes from the existence of what is called an “easy magnetization” axis within a crystal. This direction is induced by the crystallographic structure of the material studied. In the case of magnetite this easy magnetization axis is along the $\langle 111 \rangle$ direction⁸². The magnetocrystalline anisotropy energy E_{MC} corresponds to the energy needed to reverse the magnetization from this easy axis.

Another type of anisotropy that can appear in ferrimagnetic materials is the spontaneous orientation with respect to the shape of the material, it is the shape anisotropy. In any non-spherical system, the magnetization tends to align itself along the largest dimension. This energy is proportional to the square of the saturation magnetization M_s , it is often dominant compared to the other sources of anisotropy. It imposes the direction of the magnetization at equilibrium in the absence of an external field⁸².

Effect of the nanoscale on the magnetic properties of iron oxides

Superparamagnetic behavior of magnetite and maghemite at the nanoscale

If the size of the ferrimagnetic material decreases under a critical diameter D_C , creating Bloch walls requires too much energy compared to having a single domain called monodomain. The monodomain exhibits oriented magnetization along its easy magnetization axis at room temperature. We speak of “monodomain blocked IONP”. The spins inside such a blocked monodomain approach a single macrospin. Monodomain blocked IONPs display a wider opening of the hysteresis loop compared to ones with Weiss domains; they also present a remanent magnetization. The critical diameter for NPs composed of maghemite or magnetite is between 100 nm and 200 nm depending on the synthesis conditions. Esterlich J. *et al.*⁸⁵ reported diameter of 128 nm for magnetite and of 166 nm for maghemite (Figure 4).

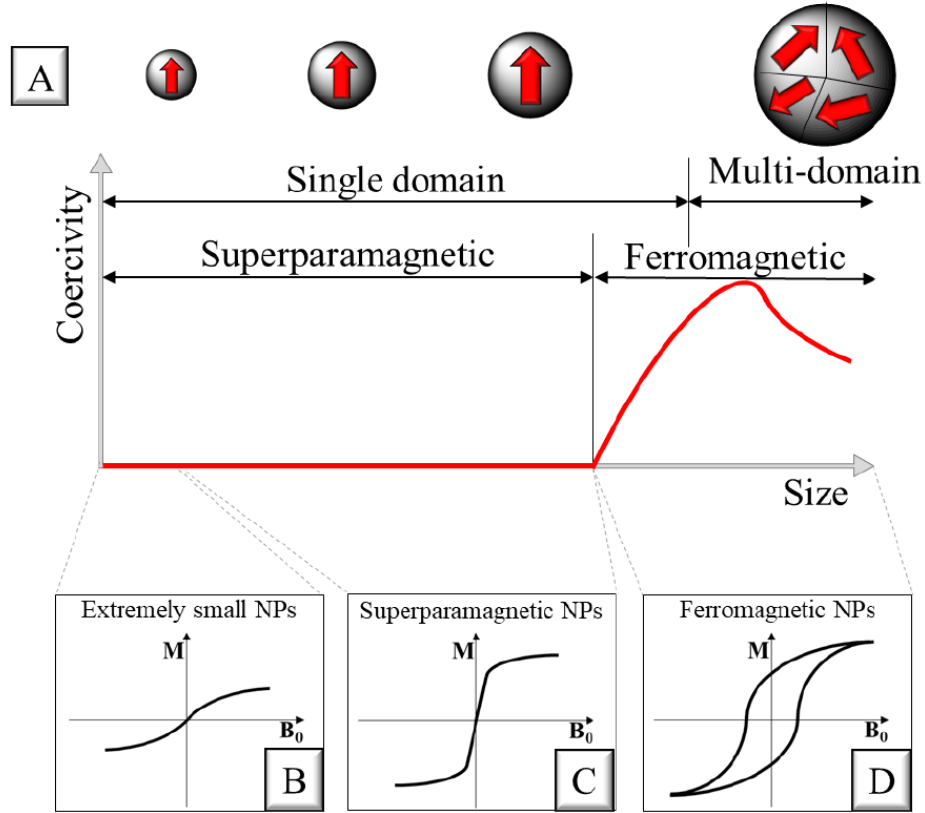


Figure 4 - (A) Evolution of coercivity as a function of the nanoparticle size. Coercivity decreases with the size of ferromagnetic materials until reaching the superparamagnetic state corresponding to single-domain nanoparticles with zero coercivity; (B-D) Magnetization curves of magnetic nanoparticles; (B) Extremely small NPs exhibit almost linear curve similar to paramagnetic substances due to very low magnetic properties; (C) Typical superparamagnetic curve of magnetic NPs with no remanence and coercivity; (D) Typical curve of ferromagnetic NPs exhibiting “magnetic memory”. Adapted from ⁸⁶.

The macrospin of NPs within monodomain has two stable positions along the easy magnetization axis (parallel and antiparallel) as depicted in Figure 5. They can switch their magnetization from one direction to the other by a movement called Néel relaxation that requires overcoming the anisotropy energy barrier KV where K is the anisotropy constant and V is the volume of the NP. For non-interacting magnetic NPs (no dipolar interactions), the probability that the magnetization spontaneously switches from one position to the other at a given temperature follows an Arrhenius law. Thus, the characteristic time for the Néel relaxation time τ_N is as follows:

$$\tau_N = \tau_0 e^{-\frac{KV}{k_B T}} \quad (I.3)$$

Here τ_0 is a length of time characteristic of the studied material, k_B is the Boltzmann constant, and T is the temperature.

When the size of the material is decreased again under a critical diameter D_{SPM} , the anisotropy energy KV becomes lower than the thermal energy $k_B T$ (Figure 5-A). The critical diameter D_{SPM} value for magnetite and maghemite depends on their synthesis method but is reported to be around 20-25 nm for magnetite and 25 nm to 30 nm for maghemite⁸⁵.

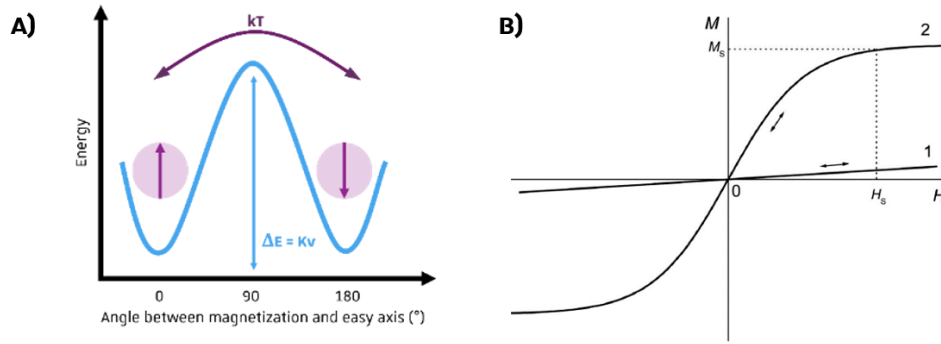


Figure 5 – A) Magnetization flip between parallel and antiparallel orientations when magnetocrystalline anisotropy energy is comparable to thermal energy; B) Schematic representation of the magnetization curve of a paramagnetic (1) material and a superparamagnetic (2) material.

As the anisotropy energy KV is lower than the thermal energy kT , magnetization can flip randomly from the two positions along the easy magnetization axis without any magnetic field applied. The material does not possess anymore a remanent magnetization at ambient temperature and the hysteresis loop is closed (Figure 5-B). The IONPs display thus a superparamagnetic behavior. The fact that superparamagnetic materials do not possess any magnetization when no magnetic field is applied is a key point for their use in biological applications. Indeed, it means that a suspension of superparamagnetic NPs won't aggregate due to magnetic interactions and can have good colloidal stability when injected *in vivo*.

When an external field is applied, the superparamagnetic material will align its magnetic moment with the field axis faster than a ferrimagnetic material as no Bloch walls are present. As soon as the external field is removed, the moments go back to a random position, giving no rise to a remanent magnetization or coercive field. Thus, when no magnetic field is applied, the material behaves like a paramagnetic material but has a high susceptibility.

Inversely, for superparamagnetic material, when the temperature is decreased below room temperature, there is a temperature from which the thermal energy becomes once again, lower than the anisotropy energy. This is the blocking temperature T_B , which is defined as follows (with τ_M the measurement time).

$$T_B = \frac{KV}{k_B \ln\left(\frac{\tau_M}{\tau_0}\right)} \quad (\text{I. 4})$$

So, under this blocking temperature T_B , the relaxation time will be higher than the measurement time thus, the magnetization will be blocked, with a magnetic moment rigidly oriented along the axis of easy magnetization. It must be noted that the blocking temperature depends on the size, the strength of the dipolar interactions, and anisotropy of the NP and the measurement time depends on the technique and apparatus used for measurement.

Effective anisotropy energy

A ferrimagnetic material can present magnetocrystalline anisotropy and shape anisotropy. But going down to the nanoscale implies a new type of anisotropy that was not present at the bulk scale: the surface anisotropy. This anisotropy is correlated to the higher ratio between atoms on the surface and in the volume of the NP.

At the surface, atoms are sub-coordinated by comparison with core atoms and due to the high surface curvature putting these atoms slightly out of equilibrium position, spins of surface atoms tend to align their magnetic moments perpendicular to the surface, which would lead to the spin canting effect (Figure 6). Indeed, when a magnetic field is applied, these spins do not align along the direction of the applied magnetic field. The spin canting phenomenon is more important when IONPs get smaller as the ratio between atoms located on the surface and those located in the core is increased. This spin canting is one reason why the saturation magnetization of IONPs is lower than that of the bulk phases. Defects and composition variation are also responsible for lower M_s values observed with IONPs by comparison with their bulk phases¹⁴.

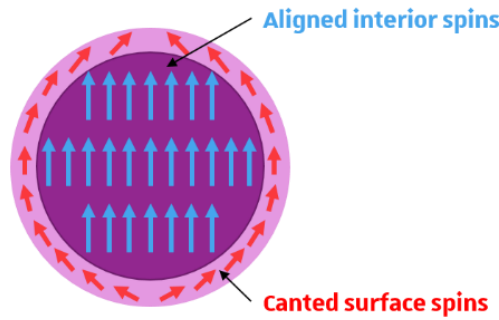


Figure 6 – Surface spin canting effect in IONPs.

With superparamagnetic IONPs, an effective energy E_{eff} is often considered, taking into account the magnetocrystalline anisotropy energy E_{MC} , the surface energy E_s and a possible shape anisotropy energy E_{Sh} :

$$E_{eff} = E_{MC} + E_{Sh} + E_s \quad (1.5)$$

Therefore, the size, the shape and the composition influence greatly the overall magnetic properties of IONPs. An increase in the NPs diameter ultimately leads to an increase of the magnetocrystalline energy, as it is proportional to KV , with V the volume of IONPs. The decrease of the surface energy with the size increase is generally overcome by the increase of energy due to the increase in NPs volume. It is also possible to change the effective anisotropy of a NP by modifying its shape. Therefore, the bigger and the more anisotropic in shape the NPs are, the higher the effective anisotropy energy is.

MRI with iron oxide nanoparticles

IONPs have been commercially used as MRI T_2 contrast agents^{87,88} and are of particular interest as biodegradable and nontoxic nano-objects compared to other contrast agents' families^{87,89}. When formulating NPs suspensions for MRI, NPs must face different issues; they must be functionalized with a ligand ensuring their colloidal stability in solution, a controlled aggregation state, an optimal diffusion of water molecules near the magnetic core, a good biodistribution, and NPs must display a high saturation magnetization⁹⁰. Hyeon's review⁹¹ demonstrated that there is still enormous potential in the NPs-based MRI contrast agents. There is currently a real need to develop these products for early, accurate, rapid and targeted diagnosis of the suspected disease and MRI is nowadays among the most used imaging techniques in clinical diagnosis.

MRI is a non-invasive medical imaging technique that allows having a 2D or 3D view of a part of the body to get access to anatomic images of soft tissues. The major advantages of this method are its non-invasiveness and its limitless depth of exploration. However, acquisition time can be long and sensitivity is sometimes weak.

MRI is based on the phenomenon of nuclear magnetic resonance of hydrogen atoms. When submitted to an intense magnetic field, the overall magnetization is parallel to its direction. When a radiofrequency field is also applied perpendicular to the external one, then the overall magnetization has two directions: longitudinal magnetization M_z (parallel to the external magnetic field), and transverse magnetization M_{xy} (perpendicular to the magnetic field). Thus, when the radiofrequency field is applied, M_{xy} increases. When it stops, the spins return to their initial state: this is a relaxation phenomenon. From this can be defined two relaxation times: longitudinal relaxation time T_1 which corresponds to the time required for the longitudinal magnetization M_z to recover toward 63 % of its initial value and the transverse relaxation time T_2 , which is the time required for the transverse magnetization M_{xy} to decrease toward 37% of its initial value (Figure 7). This T_2 called "true" comparatively to T_2^* which also take into account the inhomogeneity of the magnetic field created inside the MRI scanner. T_2^* is calculated from FID signal (Free Induction Decay) acquire by the machine during a classical MRI sequence⁹².

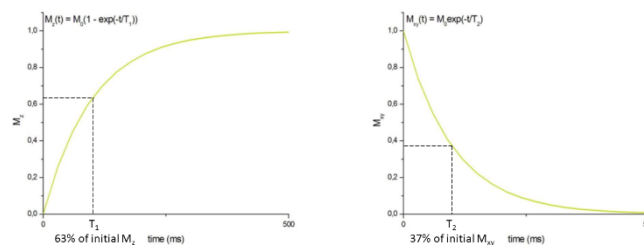


Figure 7 - Schematic representation of relaxation process with longitudinal relaxation at the left from which T_1 is the time required for the longitudinal magnetization to recover 63 % of its initial value and with transverse relaxation at the right from which T_2 is the time required for the drop of 37 % of transverse magnetization created by the frequency field.

Figure 8 explains the difference between T_2 and T_2^* . The diagram shows the process of transverse relaxation after a 90° radiofrequency pulse is applied at equilibrium. Initially the transverse magnetization (red arrow) has a maximum amplitude as the population of proton magnetic moments (spins) rotate in phase. The amplitude of the net transverse magnetization (and therefore the detected signal) decays as the proton magnetic moments move out of phase with one another (shown by the small black arrows). The resultant decaying signal is known as the Free Induction Decay (FID). The overall term for the observed loss of phase coherence (de-phasing) is T_2^* relaxation, which combines the effect of T_2 relaxation and additional de-phasing caused by local variations (inhomogeneities) in the applied magnetic field. T_2 relaxation is the result of spin-spin interactions and due to the random nature of molecular motion, this process is irreversible. T_2^* relaxation accounts for the more rapid decay of the FID signal, however the additional decay caused by field inhomogeneities can be reversed by the application of a 180° refocusing pulse⁹³. Considering that T_2^* sequences are more impacted by inhomogeneities than T_2 ones; contrast agents, such as IONPs are used on T_2^* -weighted images.

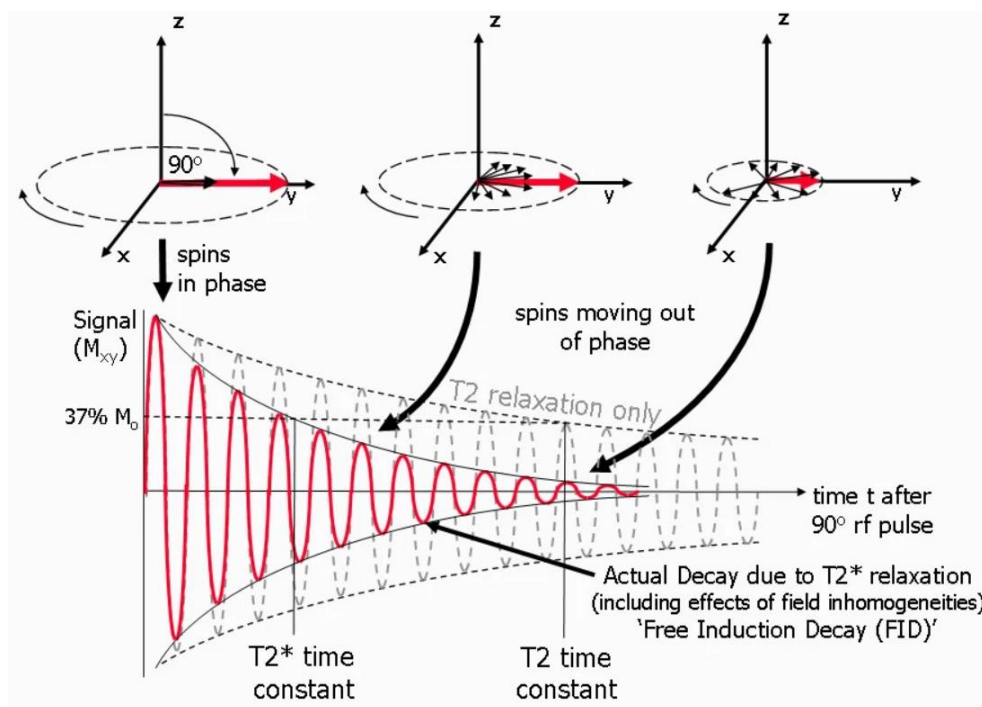


Figure 8 – Transverse (T_2 and T_2^*) relaxation process⁹³. Reprinted with permission from JCMR.

Magnetic resonance (MR) images are constructed from these relaxation processes as approximately 65 % of our body is composed of water. Contrasts are due to endogenous differences in water content in soft tissues, relaxation times, and diffusion characteristics of the analyzed tissues. The contrast can be improved by changing the parameters of the image acquisition method. However, sometimes contrast agents (CAs) are needed to increase sensitivity and help for the diagnosis. Their role is to shorten the relaxation time of surrounding hydrogen nuclei so that the contrast is increased between the areas influenced by the CA and those that are not. They give a better tissue characterization, they can reduce

image artefacts or even give a functional information. Contrast agent shorten both T_1 and T_2 , but because of their own relaxation rate which has an impact on the overall proton's relaxation rate, CAs affect more T_1 or T_2 . This is why the use of the relaxivity r_2/r_1 ratio is important, with r_x is the inverse of T_x (s^{-1}). A good T_2 contrast agent have a greater effect on T_2 than on T_1 , or a high r_2/r_1 ratio and induces a dark contrast. At the opposite, a T_1 CA have a low r_2/r_1 ratio and induce a white contrast. The diffusion of the water molecules toward the CA is also an important parameter for its effect on proton relaxation^{94,95}. In the context of molecular imaging, the specificity of MRI can be increased by directing CA to specific molecular entities.

High concentration of CA on site is needed because of the intrinsically low sensitivity of MRI (need high affinity, specificity and relaxivity). Paramagnetic Gd-complexes are T_1 CAs and IONPs have a higher effect on T_2 ^{96,97}. Some known T_1 CAs are Gd complexes due to their paramagnetic properties. Gd complexes are often used in clinic but IONPs have a better biocompatibility and are less toxic⁹⁸. Moreover, depending on their size, IONPs can be used both as T_1 and T_2 CAs. Indeed, even if the T_2 effect is still stronger than the T_1 , r_2/r_1 ratio decreases with the IONPs diameter: ultrasmall IONPs (core of 4 – 6 nm) have a stronger effect on T_1 relaxation compared to bigger ones (even if they are still used as T_2 contrasting agent)^{99,100}. Compared to paramagnetic substances, the resultant magnetic moment of superparamagnetic particles is greater and responsible for a phenomenon of magnetic susceptibility disrupting the homogeneity of the external magnetic field. Negative CA are shortening T_2 (T_2^*) much more than T_1 of the nuclei situated in their neighborhood. T_2 will be reduced through the created field gradients and T_2^* effects will appear because of field inhomogeneities leading to a signal loss in the regions capturing the contrast agent on MR images.

Several types of negative CA accumulate in the liver when intravenously injected. After binding of plasma proteins (opsonins) to their surface, Endorem (Guerbet; 4.8 – 5.6 nm core and 80 - 150 nm hydrodynamic diameter) coated with dextran, and Resovist (SHU 555A, Bayer ; 4.2 nm core, 62 nm hydrodynamic diameter) coated with carboxydextran, are captured by Kupffer cells within minutes. Since they are not retained in metastasis or hepatocytes, the darkening of liver signal (T_2) will only be observed in healthy parts of the organ, due to SPIO uptake by Kupffer cells. It is also possible to detect them in spleen and bone marrow macrophages. These IONPs were approved for detection of liver metastases in clinic before being taken off the EU and US market for economic reasons¹⁰¹. Ultrasmall particles of iron oxide (USPIO): Sinerem (Guerbet: 4 - 6 nm core + dextran coating = 20 - 40 nm hydrodynamic) has a lower r_2/r_1 ratio as compared to IONPs and are less likely to be captured by macrophages. They circulate longer, they can be used as blood pool agent for T_1 . In late phase they accumulate in liver, spleen and become potent CA for lymphography (because of their small size they can cross the capillary wall and reach lymphatic system). Metastasis do not take up USPIO, they can be used to detect lymph nodes (Clariscan, GEHealthcare/Supravist, Bayer)¹⁰². It is worth noting that most of the commercial MRI contrast agent are multicore magnetic with significant influence on their superparamagnetic behaviour^{103,104}. In case of multi-core magnetic nanoparticles, the morphology of single core is less important, in comparison with magnetic properties. Therefore, the manifold analysis of the chosen IONPs synthesis is highly relevant¹⁰⁵.

Cancer treatment with IONPs

Cancer is a global health problem that affect millions of people worldwide; with an increasing incidence. According to the Global Cancer Observatory (GLOBOCAN), cancer is the second leading cause of death globally, after ischemic heart disease; responsible for an estimated 9.6 million deaths in 2018. There are several types of cancer involving different mechanisms and with different properties or structures. Worldwide incidence, for both sexes and all ages, is given for 2020 in Figure 9. Common factor between this heterogeneous large disease family is the abnormal cell grow presenting uncontrollably divisions leading to the formation of tumors.

The best way to treat cancer is to detect tumors precociously when their progression is not too important. This is possible with screening campaign, in breast cancer context for example and efficacy diagnostic tools. This early diagnosis allow physicians to offer rapid treatment without giving chances to the tumor to develop itself or metastasis.

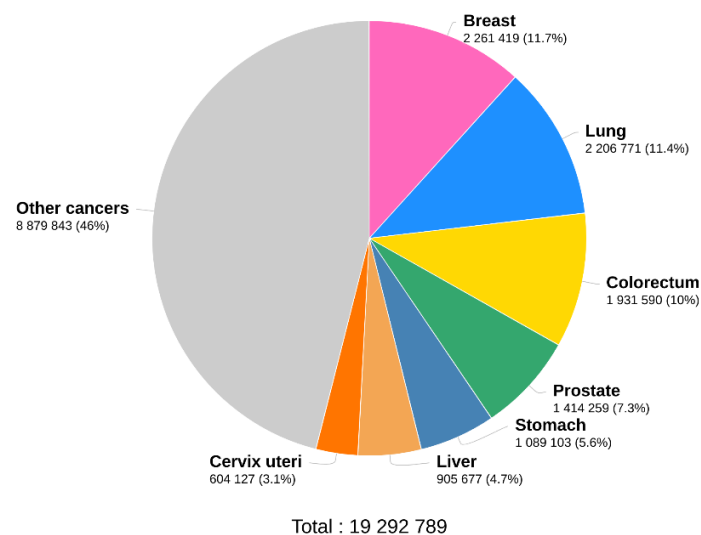


Figure 9 - Worldwide 2020 incidence for both sexes and all ages¹⁰⁶. Reprinted with permission from WHO.

Immune system's (IS) purpose is to protect an organism from diseases by distinguishing the organism's own healthy tissue from foreign organisms, such as bacteria or viruses, and unhealthy tissues such as tumoral cells. It is composed of two complementary components: the innate and the adaptative immune system¹⁰⁷. Dendritic cells and phagocytes are rapidly recruited by innate IS to recognize a pathogenic agent, digest it and eliminate cellular debris. Adaptative IS is a slower mechanism but acts specifically against recognized pathogens via B and T lymphocytes. The antigenic escape is a mechanism that occurs when a host is unable to respond to an infectious agent. Immune evasion of tumoral cells involve the tumoral micro-environment (TME) which is highly studied in this beginning of 21st century, this field is known as immune-oncology.

Tumor's development depends on the composition of TME: endothelial cells (responsible of angiogenesis), immune cells (macrophages, lymphocytes, ...), stromal cells (fibroblasts) and also acellular component such as cytokines or growth factors (*i.e.* epidermal growth factor).

Epidermal growth factor (EGF) should be noted, its receptor (EGFR) is overexpressed in many type of cancers¹⁰⁸. This receptor is involved in the tumoral proliferation induction and also in the antigenic escape of tumoral cells by inhibiting the process of presenting antigens of T-cells and down-regulating IS¹⁰⁹. TME can have various compositions regarding the tumoral type or its degree of development. It is an indicator of patients prognostic¹¹⁰.

Over the years, scientists and researchers have explored various treatment options for cancer. The chosen one will depend on the tumoral location, its stage, surgical accessibility, presence of metastasis and the patient's characteristics¹¹¹. Usual methods are surgery, radiotherapy, chemotherapy or possibly immunotherapy and targeted therapy in a uni- or multi-modal way. In the cancer context, nanomedicines know an important development, in order to enhance contrast (for diagnosis) and to treat tumoral cells while conserving healthy tissue. Indeed, Gao *et al.* have shown an increase of papers published on the subject of nanomedicine in head and neck cancer (HNC) context; mostly with pre-clinical studies¹¹², but this is verifiable for each cancer's type.

Nanoparticles designed for theranostics: “We see what we treat, and we treat what we see” (Richard Baum)

Theranostic, the integration of therapy and diagnostics has emerged as a promising strategy in cancer management. It involves the use of diagnostic tools to identify tumor. This information can then be used to select a personalized treatment approach, such as targeted drug therapy or immunotherapy. Additionally, theranostic allows for real-time monitoring of treatment response and disease progression, enabling clinicians to adjust therapy as needed. The integration of therapy and diagnostics through theranostic represents a rising approach to improving cancer treatment outcomes while minimizing side effects. As research in this area continues to advance, it is hoped that theranostic will become an increasingly used tool in the fight against cancer^{113,114}. Nanoparticles (NPs) have emerged as promising candidates for cancer diagnosis and therapy due to their unique physicochemical properties and their ability to be functionalized with targeting moieties and therapeutic agents. NPs can be designed to specifically target cancer cells, deliver drugs and other therapeutic agents to the site of the tumor and enhance the therapeutic efficacy while minimizing toxicity to healthy tissues^{115,116}. NPs are classed according to their composition, size, what they carry on and their vectorization. It is possible to give 3 nanoparticle's families: lipidic-based, polymeric-based and inorganic-based NPs. Coating, shape, size, charge and composition can be different, making any classification difficult and not exhaustive¹¹⁷ (Figure 10). Lipidic nanoparticles is the category containing the highest number of FDA (Food and Drug Administration) approved nanoparticles with mostly liposome particles. Polymeric are rarely FDA approved but seems to be nice candidates for transporting small organic molecules, biological macromolecules and proteins or vaccines. They are soluble, biodegradable but can self-agglomerate and be toxic.

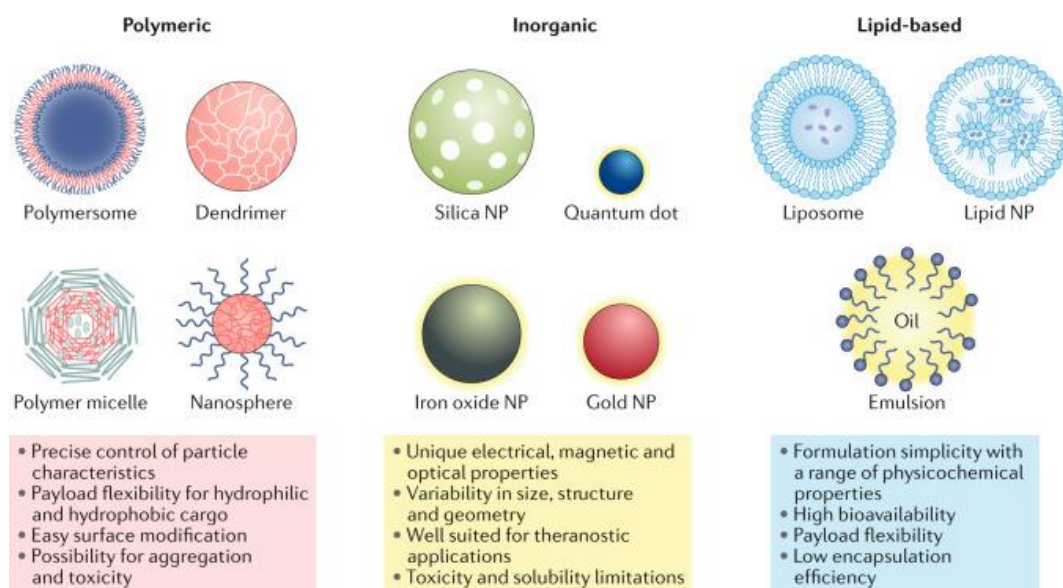


Figure 10 - Classes of nanoparticles¹¹⁷. Reprinted with permission from Nature Reviews, Drug Discovery.

Lastly, inorganic nanoparticles made of gold (GNPs), iron oxide (IONPs) or silica have been studied for various drug delivery and imaging applications. There are wide variety of structures, geometries and shapes (nano-flowers,-cubes,-pellets,-sphere, ...). IONPs have the greatest number of FDA approved bio-applications in nanomedicine among inorganic nanoparticles. IONPs have unique magnetic properties that allow them to be detected by magnetic resonance imaging (MRI). Several studies have shown that IONPs can effectively detect cancer at an early stage, including HNC. For example, a study by Attia *et al.* demonstrated that magnetic nanoparticles could increase tumoral contrast (T_2^* -weighted MR images) on mice¹¹⁸.

In order to offer a diagnosis or therapeutic ability, nanoparticles must reach and accumulate in tumoral area. After administration, they have to pass physical and biological barriers (*i.e.* epithelia, tumor micro-environment, IS) that limit the dispersal of nanoparticles. The nanoparticle's distribution will strongly impact their efficacy regardless the type of nanoparticles¹¹⁷. Their elimination is also an important issue, nanoparticles must not stay in the body for too long in order to avoid any potential toxic effect. Generally, nanoparticles are quickly eliminated by the mononuclear phagocyte system (MPS) and monocytes. A poly-ethylene-glycol (PEG) coating can increase the nanoparticle's distribution time by escaping from MPS and avoiding aggregation issues¹¹⁹. It has been shown that the size and shape of nanoparticles impact their biodistribution. Smaller ones easily cross capillaries and are quickly eliminated by kidneys compared to larger ones (> 200 nm) that activate the complement system to be quickly removed from the blood stream and seem to induce more toxicity. Furthermore, nanoparticles < 20nm have shown a higher tumoral penetration¹²⁰.

IONPs magnetic properties are known to be useful to enhance contrast on MRI, but they can also be used in therapy via magnetic hyperthermia (MH).

Magnetic hyperthermia

Iron oxide nanoparticles are able to convert electromagnetic energy into heat when they are exposed to a high frequency alternating magnetic field. This released heat can kill, or weakens, cancer cells. Hyperthermia is defined by the transient increase in temperature above 37°C. Depending on the temperature, two hyperthermic treatments have been developed: (i) mild hyperthermia, increasing temperature between 41° and 45°C, preferentially induces the death of tumor cells, according to an apoptotic process, (ii) thermoablation, for a temperature above 45°C, destroys tumors¹²¹. MH is also used to sensitize tumoral cells to another treatment, most of the time to chemotherapy^{122,123}.

During the application of an alternating magnetic field, the nanoparticles are magnetized, their magnetic moments are progressively aligned in the direction of the magnetic field by rotation. When the magnetic field is reversed, the magnetic moments relax to their new position of equilibrium¹²⁴.

Some *in vitro* studies claim that the combination of magnetic nanoparticles with an alternating magnetic field (AMF) induces cell death^{123,125–131}. SAR values are observed with increasing frequencies and/or field amplitudes. Currently, most SAR values reported in the literature are measured at a frequency range of 300 – 700 kHz and a field range of 10 – 30 kA.m⁻¹. However, for a safe application of hyperthermia to patients, a Brezovich criterion was at first established, where the product $H \cdot f$ should be less than $4.85 \times 10^8 \text{ A.m}^{-1} \cdot \text{s}^{-1}$ to avoid eddy current effects (id. to avoid non-specific heating)¹³². By taking into account further technical improvements reducing eddy current heating, Hergt and Dutz¹³³ established another criterion $H \cdot f = 5 \times 10^9 \text{ Am}^{-1} \cdot \text{s}^{-1}$ which is usually reported today. The experimental cancer models thus used have made it possible to demonstrate the concept of hyperthermia therapy using magnetic nanoparticles. Data from the literature show that it is possible to induce cell death without a detectable rise in temperature^{125,134,135}.

The challenge for *in vivo* applications is the possibility to eradicate cancer cells at the tumor site without damaging adjacent normal cells. Thus the pharmacokinetics, toxicity and biodistribution of nanoparticles are very important¹³⁶. Several groups have studied magnetic hyperthermia in rodents and rabbits. A few human clinical trials have also been conducted^{137–139}. NP administration consists either in injecting a NP suspension directly into the tumor, or intravenously, before applying the magnetic field. The validation of the concept of magnetic hyperthermia was first carried out by directly injecting the nanoparticles into the tumor. This approach allows to control the amounts of nanoparticles injected and to use relatively high doses compared to other modes of injection.

As we seen, in cancer context, one main challenge of theranostic nanomedicine is the specific targeting. The therapeutic distribution (drugs, heat, ...) must be focalized in the tumoral neighboring in order to be fully efficient and to decrease the side-effect probability. Tumoral micro-environment must be taken into account because of the non-homogeneous and abnormal vasculature around tumors¹⁴⁰. Two approaches exist in the delivery of nanoparticles: passive and active targeting.

Targeting strategies

A major challenge in nanomedicine is to design NPs able to accumulate specifically in tumoral tissues without accumulating in clearance organs like the liver, the spleen, or the kidneys. There are two main mechanisms reported for the uptake of theranostic nanoplateforms in tumor sites. The first one is called “passive targeting”, this targeting occurs because NPs, due to their size (diameter inferior to 100 nm) can pass easily through the abnormal vasculature of tumors. Indeed, they generally present irregular fenestrations and poor lymphatic drainage compared to healthy tissues. We talk about the enhanced permeability and retention (EPR) effect^{118,141}. However, the effectiveness of this effect depends on the tumor microenvironment but also on the capacity of NPs to accumulate there. Moreover, after intravenous (i.v.) injection, most developed NPs tend to accumulate in phagocytic organs such as the liver, spleen, and kidneys, and only small amounts are seen accumulated in tumors, as for example for iron oxide-based NPs^{142–144}. Because of this limitation, a lot of research was done to develop “active targeting”. The purpose is to selectively reach abnormal tissue, avoiding the uptake of NPs by healthy tissues. In this sense, the active targeting consists firstly in finding a receptor overexpressed in the type of cancer of interest. Once the target is defined, a specific molecule, known as the targeting ligand (TL), can be used to deliver the NPs directly to this site. These two modalities are resumed in the Figure 11^{145–147}.

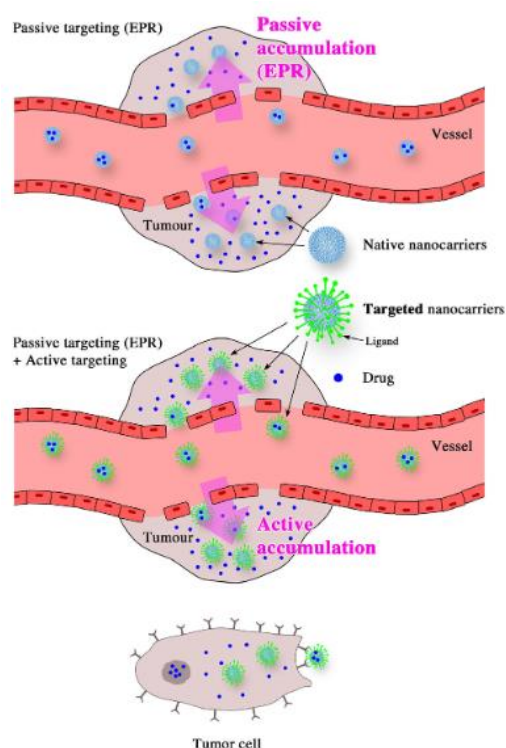


Figure 11 - Scheme illustrating the passive targeting by EPR effect and the active targeting into tumor site (Attia et al.¹¹⁸). Reprinted with permission from Oxford University Press.

It is worth nothing that the cellular internalization could be passive or active, depending on the presence of targeting ligands and can be modified by the shape or the size of nanoparticles. A passive diffusion through membrane is possible for smaller particles, but an active transport is mandatory for bigger ones.

Passive targeting

EPR effect was discovered in 1980s by Maeda *et al.* It is the physiology-based main mechanism for large molecules and small particles to accumulate in tumors¹⁴¹. The blood vessels endothelium is fenestrated (200 - 800 nm) and becomes more permeable under certain conditions, such as inflammation or hypoxia, which is typical of tumor. Hypoxia promotes the formation of new blood vessels or the engulfment of existing ones by rapidly growing tumors. These newly formed vessels are leaky, allowing for selective enhanced permeation of macromolecules larger than 40 kDa and nanosystems to the tumor stroma. New vessels do not present a normal lymphatic drainage that contributes to the retention of NPs^{148,149}. Small low-molecular-weight agents, because of their ability to return to the circulation by diffusion, are not retained in tumors. Furthermore, the accumulation in tumoral site depends on nanoparticle's physico-chemical properties, such as size, surface charge and coating. The optimal NPs size range is around 20 - 200 nm to favor EPR effect. Particle diameter has a significant impact onto their biodistribution, as seen previously^{150,151}. Uptake by the MPS is a significant disadvantage in most therapeutic applications; a way to reduce the macrophage uptake is to coat nanoparticles with a hydrophilic polymer such as PEG which helps to reduce their opsonization by plasma protein¹⁵². We can cite Doxil® and Caelyx®; two pegylated liposomal drugs (doxorubicin) delivery system used in clinic that passively target breast and ovarian metastatic tumors.

Active targeting

Among the most used receptors are the folate receptor, which can be targeted with folic acid on the surface of NPs¹⁵³ or the Human Epidermal Growth Factor Receptor 2 (HER2+) which is recognized by the monoclonal antibody Trastuzumab for example¹⁵⁴. Peptides, nano-bodies, affibodies, proteins, small organic molecules, or nucleic acids constitute examples of short TL grafted to NPs^{143,155–159}. The large antibodies or the smaller versions of them, the fragment antigen-binding (Fabs), are also common TL¹⁶⁰. Iron oxide nanoparticles (IONPs), which accumulate in tumors without TL via intratumoral injection or passive targeting as a result of the EPR effect, are among the most developed and promising NPs at the moment^{144,145,147,161–165}. When magnetic properties of the NPs are involved, another way to increase their accumulation is to apply a magnetic targeting, in which a magnetic field gradient guides IONPs toward the tumor; the main drawback of this technique is the requirement of a magnet that should be positioned easily near the tumor, thus limiting this strategy to specific cases. In this context, active targeting appears as a promising way for NPs selective internalization. However, Wilhem *et al.* observed that just 0.7 % (median) of the i.v. administered nanoparticle dose (with or without TL) was found to be delivered to solid tumors after reviewing the literature from the previous 10 years¹⁴⁴. Similar low percentages of internalized IONPs were also reported by Alphandery *et al.*, who showed that many of them were accumulated in the liver and kidneys¹⁶². Therefore, there is a strong need to further understand how active targeting can be improved to increase the percentage of accumulated NPs in tumor sites after i.v. injection. This implies a better understanding of the key parameters that must be improved to raise the efficacy of IONPs bearing TL as active targeting systems. Among these parameters, the choice of the TL is essential. It is not an easy choice as it must target overexpressed

receptors at the surface of cancer cells only. Moreover, the size of the TL must be suitable to the mean size of IONPs and the grafted TL must conserve its recognition capacity toward its target, a fact that imposes *sine qua non* conditions on the chosen bioconjugation approach to avoid the involvement of the active site in the coupling. In the case of short TLs, a major concern is to avoid abrupt changes in the 3D conformation of the molecule (upon conjugation to the NP) that may alter its interactions with the cellular receptors. Lastly, the TL must remain fully exposed to the solution and not buried inside the organic coating (such as PEG chains) already present on the IONPs surface. The coupling of the TL at the surface of IONPs is also an important step. There is a wide spectrum of bioconjugation reactions¹⁶⁶ used to attach TL at the surface of functionalized IONPs and; globally they can be divided into two types: covalent or non-covalent conjugations. The first group belongs to the carbodiimide chemistry¹⁶⁷, Michael addition¹⁶⁸, click Chemistry¹⁶⁹, or Diels-Alder cycloaddition^{143,170}, among others. In non-covalent conjugation, the most common ones are electrostatic interactions, metal affinity coordination, or biotin-avidin interaction¹⁷¹. The choice of reactions mainly depends on the type of molecule used as a TL and its eventual functional group that may be used to perform a covalent conjugation technique, which brings more stability for the grafting than a non-covalent technique. Furthermore, it is also important to validate the presence of TL at the surface of IONPs and to quantify it¹⁷².

Commonly, the presence of TL at the surface of IONPs may be checked by FTIR spectroscopy or thermogravimetric analysis (TGA) if the amount of TL is high enough, but most of the time it is determined by the observation of an increase in the hydrodynamic size or a change of zeta potential values. Hence, the most challenging step is the quantification of the amount of TL at the surface of IONPs^{147,155,158,173}. The active endocytosis pathway can pass through clathrin- or caveolin- mediated but also endocytosis without mediation. Clathrin involves the formation of vesicles after ligand-receptor contact. Caveolin takes part in the protein, lipidic and fatty acid regulation¹⁷⁴. Svitkova *et al.*¹⁷⁵ have shown that bovine serum albumin (BSA) coated nanoparticles are mostly internalized by clathrin mediated endocytosis but PEG coated ones use caveolin and lipid raft for their internalization. EGFR has been introduced earlier as a good receptor to target for cancer uses because of its overexpression in tumoral cells and its implication in angiogenesis and tumorigenesis process. Study have shown that small molecular weight peptide presents a good affinity to EGFR¹⁷⁶.

Magnetic drug targeting is another way to actively target tumors. Using superparamagnetic properties of IONPs, nanoparticles are guided through the body under the action of a localized magnetic field to specifically deliver therapeutic effects. Magnetic nanoparticles with high saturation magnetization responds better to the magnetic field, allowing an higher tumoral accumulation. It will strongly depend on the size and shape of nanoparticles^{6,177}. Freeman *et al.* (1960)¹⁷⁸ where firsts to use magnets to move iron particles through vascular system. More recently, Shen *et al* (2015)¹⁷⁹ has proved a higher IONPs retention in the rat's heart when placed under localized external magnetic field. This retention seems to be proportional to the magnetic field strength.

With this better understanding of the biodistribution and internalization pathway of nanoparticles from the administration to the target; some examples of interesting multimodal nanoparticles will be presented in the next part.

Multimodal nanoparticles

Multimodal nanoparticles are nanoparticles that have physico-chemical properties allowing diagnosis and/or therapeutic effect, such particles can carry multiple types of payloads, such as drug, imaging agents, and targeting ligands in a single particle. By definition theranostic nanoparticles are multimodal. These nanoparticles can offer several advantages over traditional cancer therapies, including improved targeting of cancer cells, enhanced drug efficacy, delimitation of tumors and reduced side effects. Figure 12 presents the different applications for IONPs. In recent years, the development of multimodal nanoparticles has gained significant interest in the cancer research community for their therapeutic and diagnostic applications allowing for real-time monitoring or drug delivery and tumor response¹⁸⁰.

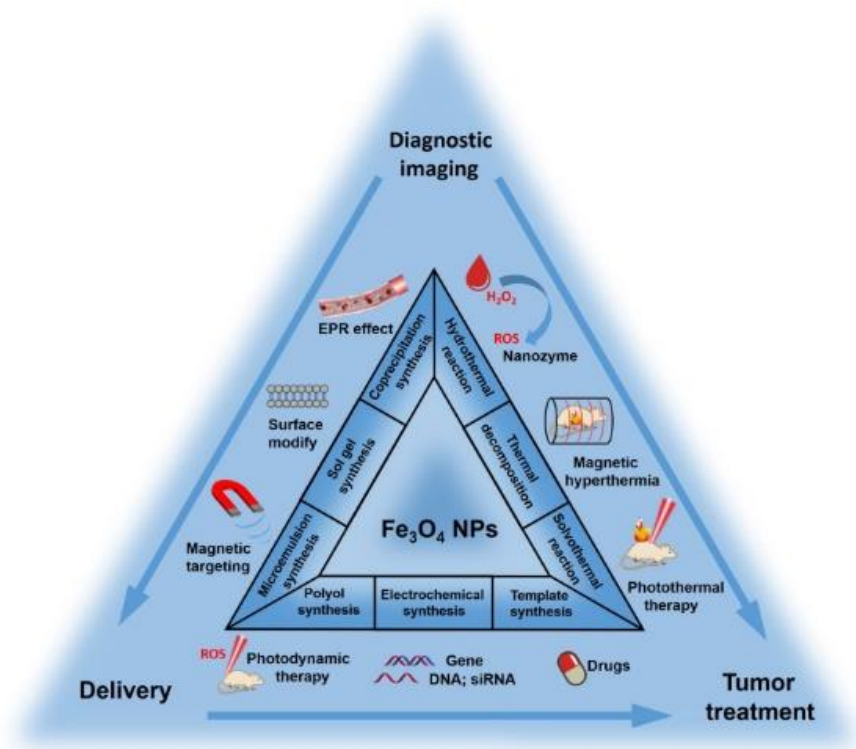


Figure 12 – IONPs applications in cancer diagnosis and treatment¹⁸⁰. Reprinted with permission from *Theranostics*.

In this context, understanding the properties and behavior of these NPs in biological systems is a key point for their successful translation into the clinic. In this part, several examples of nanoparticles classified by therapeutic effect will be seen.

Radiotheranostic

Radiation therapy (RT) is the main way to treat cancer, approximately 50 % of all cancer patients receive radiation therapy¹⁸¹. This treatment uses high-energy radiation to kill cancer cells. It can be delivered by external beam (X-ray) or internal radiation therapy (brachytherapy) which involves placing a radioactive source inside the body, near the tumor. These radiations damage DNA and biological macromolecules, preventing cell proliferation and tumor growth. Healthy cells are impacted by these radiations but are, usually, more able to repair themselves and recover from the damages. Radiation therapy is often used in combination with surgery or chemotherapy to prevent resistance or tumoral recurrence. This is a non-specific treatment but always localized in the tumoral region. Despite the recent progress of radiation therapy with thinner ionizing beam, dose fragmentation, or Flash (ultra-high dose rate radiation); a lot of research are in course to reduce side-effects by decreasing the dose or by increasing the tumoral sensitivity to RT or to deliver in a very localized way radiation inside the tumor.

The aim of NPs combination with X-rays radiotherapy (XRT) or proton-therapy (PRT) is to potentialize irradiations effects and to increase specificity in order to decrease the distributed dose and spare surrounding healthy tissues. Many metallic nanoparticles have been studied for these application because of their high atomic number (Z) increasing the probability to interact with radiations^{182,183}.

Hainfeld *et al.* in 2004¹⁸⁴ were the firsts to develop gold nanoparticles to enhance radiotherapy in mice. They irradiated mice bearing subcutaneous mammary carcinomas with X-rays with and without pre-injection of GNPs. One-year survival was 86 % for mice injected with GNPs versus 20 % for the control group irradiated with the same energy. It shows the interest of GNPs combined with XRT. Furthermore, there was no apparent toxicity for mice, and GNPs were largely cleared from the body through the kidneys. More recently, Li *et al.*¹⁸⁵ have functionalized polyallylamine-coated GNPs with Cetuximab, a monoclonal antibody targeting and blocking epidermal growth factor receptor (EGFR), thus inhibiting the tumoral development. For the first time, an enhanced cellular uptake, thanks to Cetuximab combined with radio-enhancing effect was successfully tested *in vitro*. Figure 13 shows the direct damages to DNA by photon (red wiggly line) and ion (red straight line) radiations; but also mitochondria. The impacted medium produces secondary electrons, radicals and reactive species that will also impact DNA, organelles and macromolecules (indirect damages)¹⁸³.

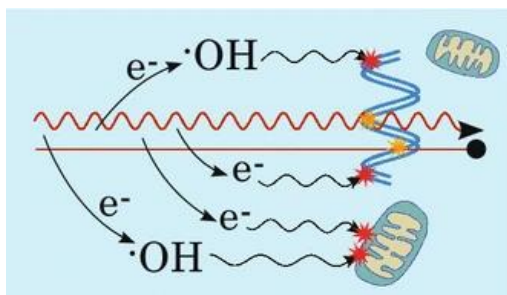


Figure 13 – Illustration of radiation damage mechanisms ¹⁸³. Reprinted with permission from *Cancer Nanotechnology*.

Tumor radiosensitization was also studied on iron oxide nanoparticles (IONPs) irradiated by gamma-radiation by Shetake *et al.* (2019)¹⁸⁶. After nanoparticles injection, the tumoral growth was significantly decreased. Furthermore, this kind of NPs have the advantage to induce a T_2^* -weighted MRI contrast which allows their monitoring inside the patient's body. Ahmad *et al.*¹⁸⁷ have compared the radiosensitizing effect of three commercially available NPs (GNPs, IONPs and Gd-complex) on tumoral cells (MCF-7 and U87). After measuring the NPs uptake and cytotoxicity; they shown a higher enhancement factor (radiosensitizer effect) with GNPs on U87 and no difference on MCF-7. IONPs main advantage is to be monitored directly in the patient's body via MRI.

Ternad *et al.* (2023) have studied IONPs radiosensitizing properties¹⁸⁸ on tumoral cells (A549) exposed to 225 kV X-rays. As results, authors describe that radiosensitization does not result only from a physical phenomenon but that an important part comes from biological events. They demonstrated an inhibition of thioredoxin reductase enzymes that prevent the regeneration of intracellular antioxidant and have a role in the management of oxidative stress. Inhibiting these proteins increase the effect of the radiation therapy by preventing cells from self-repairing.

Chemotherapeutic nanoparticles

Chemotherapy is a main treatment option for cancer after surgery even if side-effects have been reported since the beginning of its use on tumors in the 1940s by Louis S. Goodman and Alfred Gilman. It is a treatment that uses chemicals to destroy cancer cells in the patient's body. Chemicals used have as main target cells that divide and grow rapidly; which is the case for tumoral cells. These drugs work by interfering with the cell division process and prevent it. Chemotherapy is usually given in cycles, with a period of treatment followed by a period of rest to allow the body to recover. Indeed, this is a non-specific, or a systemic, treatment that attacks every dividing cells, which causes many side-effects and decrease significantly the patient's quality of life. Chemotherapy is often combined with other treatment such as surgery or radiation therapy because of the potential chemo-resistance of tumoral cells, furthermore, several drugs are frequently administered extemporaneously with different modes of operation¹⁸⁹. Depending on the location of the tumor, the combination of drugs is different. For example in lung cancer, it is recommended to deliver cyclophosphamide, doxorubicin, vincristine and prednisolone but for colorectal cancer, 5-fluorouracil, folic acid and oxaliplatin are prescribed¹⁹⁰. Despite the efficacy of chemotherapy, it is not used for every patient

because of chemo-resistances which can occur due to various factor such as genetic mutations, tumor-microenvironment, or the type of tumoral cells. Intrinsic resistance is the resistance due to the tumor type, for example triple negative breast cancer has a decreased responsiveness to drugs. We can also quote gastric cancer overexpressing HER2 that are known to be resistant to cisplatin¹⁹¹. Acquired resistance is a gradual reduction of anticancer efficacy of a drug during treatment. It may result of mutation due to the drug, a second proto-oncogene activation or changes in TME after treatment. As example, neuroblastoma cancer cells release exosomes to the TME that induce production of miRNAs by tumor-associated macrophages (TAMs) after cisplatin treatment. These miRNAs will silence the TERF1 gene of neuroblastoma cells, increasing their telomerase activity and their resistance to chemotherapy¹⁹². A scheme of some resistance mechanisms examples is given in Figure 14¹⁹³.

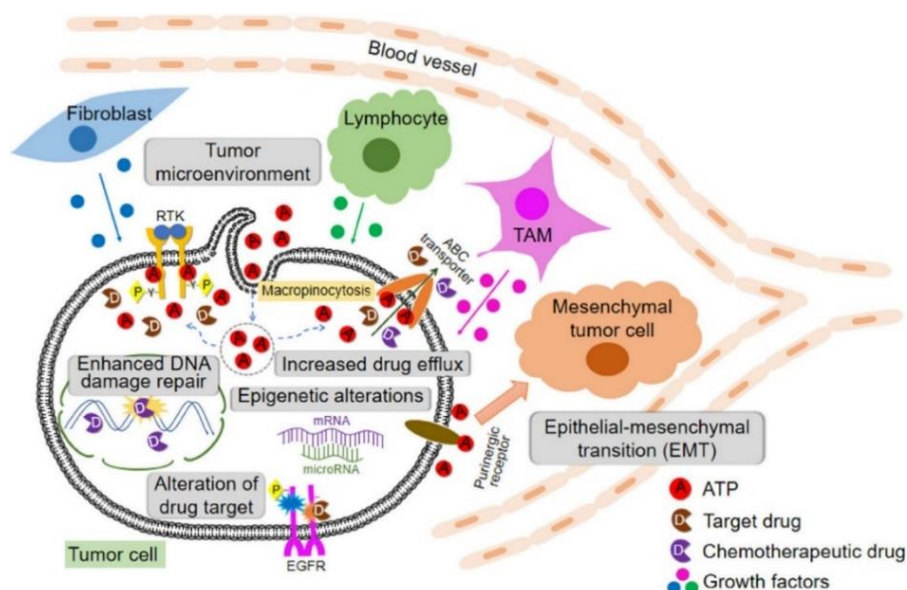


Figure 14 - Cancer cells mechanisms involved in drug resistance¹⁹³. Reprinted with permission from *Cancer Nanotechnology*

Therefore, there is a need to develop new strategies to deliver chemotherapeutic drugs in tumoral cells that are resistant or have developed a resistance and also to deliver them locally in order to reduce side-effect by decreasing the concentration in the body. In this context, nanoparticles seem to be good candidates.

Huang et al. (2017) develop IONPs co-coated with PEG and PEI polymers design for dual target-specific drug delivery and MRI in cancer theranostic¹⁹⁴. Targeting part of these NPs is supported by conjugation of folic acid which receptor is overexpressed in various human carcinomas. IONPs are here loaded with doxorubicin and injected on MCF-7 tumoral xenografted mice. Authors describe a nice IONPs tumoral uptake but with a predictable accumulation in the liver. The efficacy of this drug-delivery system was proven by a stable tumoral growth 35 days post-injection for the group Dox-loaded IONPs and also by the increased presence of IONPs in tumors *ex vivo* for NPs conjugated with folic acid compared to NPs without targeting ligand. Smart nanocarrier for multi-stimuli on-demand drug delivery have also been synthesized by Elsami et al. (2022)¹⁹⁵. Flower-like IONPs were encapsulated in a dual pH and thermoresponsive responsive copolymer to release drugs (Dox.) in a highly

controlled way. A negligible amount of doxorubicin was released from nanoparticles in physiological conditions (37°C and neutral pH). But increasing the temperature and decreasing pH by magnetic hyperthermia, Dox. was massively released from NPs in their surrounding environment; suggesting that IONPs can be used to remote-control drug release in combination with MH for cancer treatment.

El-Dakdouki's team develop hyaluronan-coated iron oxide nanoparticles (HA-IONPs) loaded with doxorubicin for preclinical. Hyaluronan was chosen to target CD44, a cell surface glycoprotein expressed on many cancer cells. An accumulation of NPs; darkening inside the yellow circle is observed on tumoral mice (Figure 15) 1h post-injection and still observable 24h after. The injection of Dox-HA-IONP inhibits the tumoral growth approximately 4 times more than free doxorubicin. Efficacy is proved to be higher than standard Dox even with an inferior doxorubicin concentration (2 mg_{Dox}/kg_{body} for condition Dox-HA-IONP versus 8 mg_{Dox}/kg_{body} for the condition free Dox.) implying less side-effects^{196,197}.

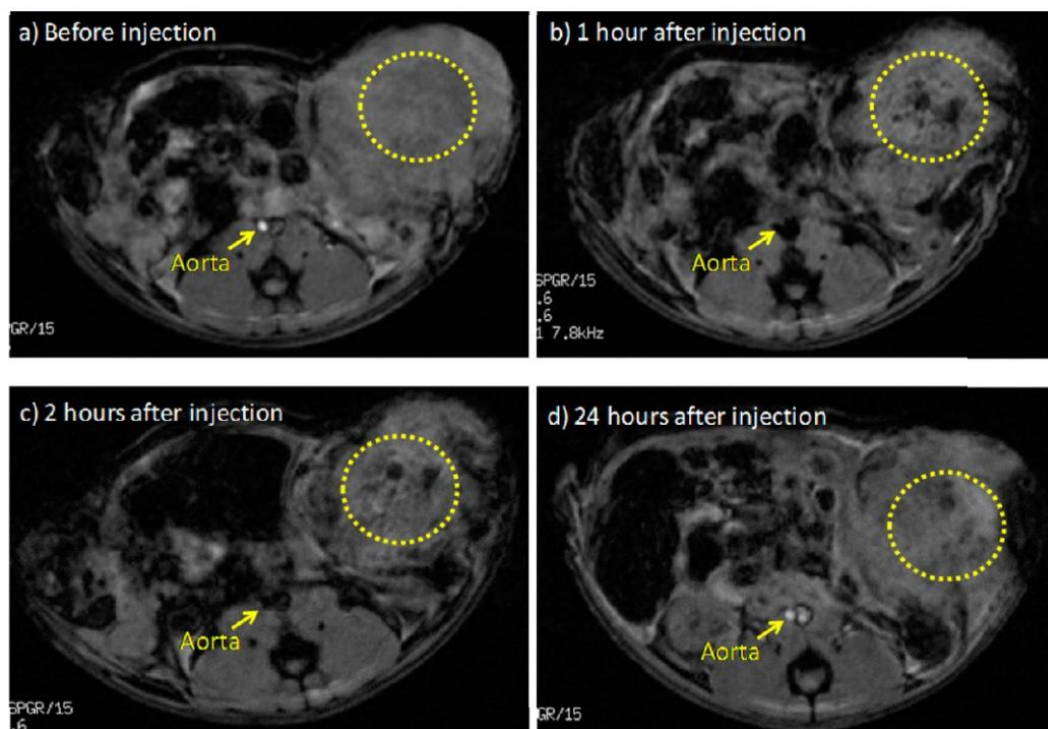


Figure 15 - T_2^ -weighted MR images of mouse tumor before injection, 1h, 2h and 24h after HA-IONP injection. Negative contrast is highlighted in yellow circle suggesting the presence of IONPs¹⁹⁷. Reprinted with permission from ACS.*

Some nanoparticles are tested in clinical study as drug delivery system; because of their biocompatibility, lipidic-based NPs are the firsts to reach this step. These studies will serve as proof-of-concept for IONPs drug delivery system. We can cite the phase II clinical study, on 98 Korean women presenting ovarian cancer, Lee et al (2007) have used cremophor-free polymeric micelle with paclitaxel as first-line treatment¹⁹⁸. They compared the efficacy of their micellar formulations of paclitaxel to a generic treatment with paclitaxel. As conclusion, they showed a non-inferior efficacy and less side-effects because of the presence of micelles enhancing solubility of paclitaxel and allowing a higher accumulation of drugs on tumoral site.

Magnetic hyperthermia activated drug delivery

As shown previously in this chapter, magnetic nanoparticles enable specific response when submitted to high frequency (magnetic hyperthermia) or low frequency (magneto-mechanical therapy) alternating magnetic field (AMF). As other metallic nanoparticles, they produce reactive oxygen species, intrinsically or under ionizing beam, making them interesting for cancer treatment.

Guisasola *et al.* (2018) used IONPs embedded in a mesoporous silica matrix and coated with an engineered thermoresponsive polymer. Under AMF, temperature increase in the NPs neighboring causing the polymer transition and the consequent release of drug (Doxorubicin) trapped inside the silica pores. The therapeutic efficacy is not based on the tumoral tissue heating which avoids the necessity to employ large amount of magnetic cores as is common in current MH. Furthermore, the chemotherapeutic agent is delivered in the tumoral region decreasing the side-effect risk¹⁹⁹. The tumoral growth monitored is significantly decrease for the condition: magnetic hyperthermia + doxorubicin compared to conditions MH or Dox. alone. The combination of both treatments (chemotherapy and MH) confers a higher efficacy and less side-effects.

In 2021, Fang *et al.*²⁰⁰ have developed magnetic liposomal systems conjugated with a targeting ligand and loaded with a immunotherapeutic drug (CSF1R inhibitor). The combination of MH and M2 macrophage repolarization in tumoral microenvironment relieves tumoral immunosuppression, normalizes tumor blood vessels and promotes the infiltration of T-lymphocytes. After the treatment, an increase of antitumoral effector CD8⁺ T cells was also observed. Thus, TME was remodeled, nanoparticles have also activated immune response and memory inhibiting tumoral recurrence.

Photoresponsive nanoparticles

Development of photosensitizers multimodal NPs in the cancer therapy context is a topic in expansion. Upon UV-vis or near-infrared (NIR) light, metallic nanoparticles can heats their surrounding environment²⁰¹. Figure 16-a) illustrates the production of reactive oxygen species (ROS) due to photochemical reactions with oxygen after exposure to UV light, this mechanism is known as photodynamic therapy (PDT). On Figure 16-b), the photothermal therapy (PTT) is represented; after irradiation with NIR light, nanoparticles heat surrounding cells. Both techniques are minimally invasive but have a major limitation, the low light penetration through tissues²⁰². The first team that has shown the conversion of light absorbed by IONPs to local heating was Yu *et al.* (2011)²⁰³. Under NIR irradiation, alumina-coated iron oxide magnetic nanoparticles were used as photothermal agents to selectively kill bacteria. After 5 min of light irradiation, the temperature increased by 20 °C and decreased nosocomial bacteria growth (Gram positive and negative and antibiotic-resistant) by over 95% within 10 min of light irradiation. The possibility to do PTT with nanoparticles was also proved on highly crystallized iron oxide nanoparticles coated with polysiloxane-containing copolymer²⁰⁴ offering great antibiofouling properties and an enhanced tumoral accumulation through EPR effect. Different composition were successfully tested to induce PTT, such as carboxymethyl chitosan-coated or PEGylated IONPs; or plasmonic MXene-based nanocomposites^{204–208}.

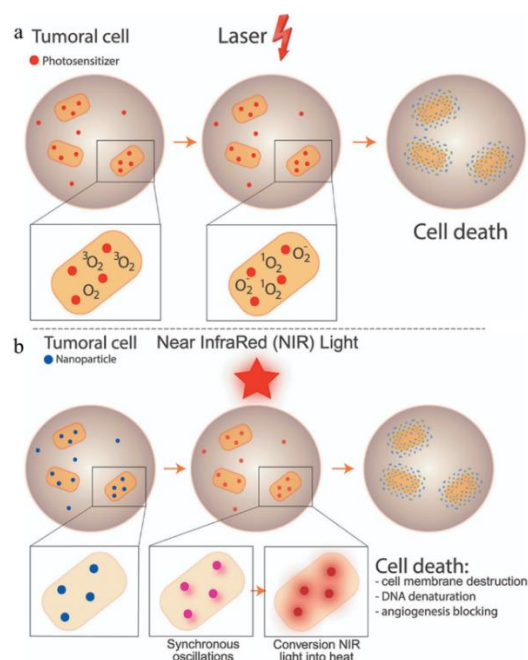


Figure 16 - Illustration of (a) photodynamic therapy and (b) photothermal therapy mechanisms²⁰⁹. Reprinted with permission from De Gruyter.

Besides the possibility to heat or produce ROS after illumination, nanoparticles able to release drugs upon exposure to light have been developed. Wu et al (2017) have loaded IONPs with doxorubicin via thermos-sensitive bond, cleaved by a near infrared exposure²¹⁰. Using magnetic targeting, NPs are accumulated inside tumors; photothermal therapy is activated upon NIR exposure and doxorubicin is released. These nanoplatforms were tested on MCF-7 and on xenograft tumor Balb/c nude mice. Tumoral growth was significantly decrease using the combination of PTT and doxorubicin delivery compared to other groups. Sun et al. (2019) have also demonstrated the interest of using IONPs as chemo-photodynamic combination therapy²¹¹. Authors used an aptamer-hybridized nucleic acid structure to target tumoral cells; and IONPs were loaded with a chemical anticancer drug: daunomycin and a photosensitizer molecule. Upon visible light, PDT mechanism induces ROS production and daunomycin is released the tumoral micro-environment. They showed *in vitro* an accurate tumor targeting and high cytotoxicity after light exposure.

NIR illumination can also serve for real-time imaging. Kanwar et al. (2016) used iron oxide saturated lactoferrin nanocapsules (FebLfNCs) for real-time imaging and anti-tumoral therapy. Iron saturated form of lactoferrin have outstanding immune-modulatory properties: interleukins productions, activation of macrophages, natural killer (NK) cells, dendritic cells. FebLfNCs are emit fluorescence (675-740 nm) after NIR light exposure. Authors conclude in an efficacy drug-delivery system that can be monitored *in vivo* on tumoral mice model with NIR fluorescence imaging. It could be interested to implement PTT or PDT to this kind of theranostic nanoplatforms in order to increase its therapeutic ability. Many preclinical studies can be found on the use of nanoparticles in photothermal therapy, it is possible to cite Wu et al. working on the combination of hyperthermia and drug-release with pegylated silica-core gold nanoshells exposed to an external NIR laser irradiation²¹². But few examples have reached clinical trial.

Conclusion

The synthesis and characterization of iron oxide nanoparticles (IONPs) have been the focus of intense research due to their unique magnetic properties and potential applications in a wide range of fields, including biomedical, environmental, and industrial areas.

On this chapter, the synthesis and characterization of IONPs have been studied. The ability to control their size and shape using various synthesis methods has been a key aspect of their development, as it allows for the fine-tuning of their physico-chemical properties. One of the main applications of IONPs is in magnetic resonance imaging (MRI) where these properties can be exploited to enhance contrast and improve the sensitivity and specificity of this imaging tool. IONPs also shown a great potential as theranostic nanoplatforms. Magnetic hyperthermia (MH) uses IONPs to selectively heat tumor tissue, leading to the destruction (or weakening) of tumoral cells. An explanation of this therapy was given here and various parameters have been identified to optimize IONPs magnetic properties for improved cancer diagnosis and therapy.

An overview of the cancer problematic was given; introducing the main challenges of tumoral treatments (surgery, chemotherapy and radiation therapy). Main issue of nanomedicine is to target tumoral cells. An overview of passive and active targeting was given here, with a highlight for magnetic drug targeting. Specific targeting is a key point to increase anti-tumoral efficacy and decrease side-effects. Currently, various IONPs nanoplatforms are developed notably for diagnostic: MRI, radiolabeled for PET/SPECT (Positron emission tomography and Single-photon emission computed tomography) or real-time monitoring under near-infrared exposure; and therapeutic: MH, photodynamic (PDT) and photothermal therapy (PTT) or as drug delivery system.

References:

- 1 S. M. Dadfar, K. Roemhild, N. I. Drude, S. Stillfried, R. Knüchel, F. Kiessling and T. Lammers, *Advanced drug delivery reviews*, 2019, **138**, 302–325.
- 2 A. Ali, H. Zafar, M. Zia, I. ul Haq, A. R. Phull, J. S. Ali and A. Hussain, *Nanotechnol Sci Appl*, 2016, **9**, 49–67.
- 3 X. L. Dong, C. J. Choi and B. K. Kim, *Journal of Applied Physics*, 2002, **92**, 5380–5385.
- 4 R. Massart, *IEEE Transactions on Magnetism*, 1981, **17**, 1247–1248.
- 5 W. Ling, M. Wang, C. Xiong, D. Xie, Q. Chen, X. Chu, X. Qiu, Y. Li and X. Xiao, *Journal of Materials Research*, 2019, **34**, 1828–1844.
- 6 D. Stanicki, T. Vangijzegem, I. Ternad and S. Laurent, *Expert Opin Drug Deliv*, 2022, **19**, 321–335.
- 7 T. Hyeon, S. S. Lee, J. Park, Y. Chung and H. B. Na, *J Am Chem Soc*, 2001, **123**, 12798–12801.
- 8 S. Sun and H. Zeng, *J Am Chem Soc*, 2002, **124**, 8204–8205.
- 9 C. B. Murray, D. J. Norris and M. G. Bawendi, *J. Am. Chem. Soc.*, 1993, **115**, 8706–8715.
- 10 X. Peng, J. Wickham and A. P. Alivisatos, *J. Am. Chem. Soc.*, 1998, **120**, 5343–5344.
- 11 V. K. LaMer and R. H. Dinegar, *J. Am. Chem. Soc.*, 1950, **72**, 4847–4854.
- 12 Y. Xia, Y. Xiong, B. Lim and S. E. Skrabalak, *Angew Chem Int Ed Engl*, 2009, **48**, 60–103.
- 13 S. G. Kwon, Y. Piao, J. Park, S. Angappane, Y. Jo, N.-M. Hwang, J.-G. Park and T. Hyeon, *Journal of the American Chemical Society*, 2007, **129**, 12571–12584.
- 14 W. Baaziz, B. P. Pichon, S. Fleutot, Y. Liu, C. Lefevre, J.-M. Greneche, M. Toumi, T. Mhiri and S. Begin-Colin, *J. Phys. Chem. C*, 2014, **118**, 3795–3810.
- 15 Y. Xia, Y. Xiong, B. Lim and S. E. Skrabalak, *Angewandte Chemie (International ed. in English)*, 2009, **48**, 60–103.
- 16 F. Pertion, G. Cotin, C. Kiefer, J.-M. Strub, S. Cianferani, J.-M. Greneche, N. Parizel, B. Heinrich, B. Pichon, D. Mertz and S. Begin-Colin, *Inorg. Chem.*, 2021, **60**, 12445–12456.
- 17 H. Chang, B. H. Kim, H. Y. Jeong, J. H. Moon, M. Park, K. Shin, S. I. Chae, J. Lee, T. Kang, B. K. Choi, J. Yang, M. S. Bootharaju, H. Song, S. H. An, K. M. Park, J. Y. Oh, H. Lee, M. S. Kim, J. Park and T. Hyeon, *J. Am. Chem. Soc.*, 2019, **141**, 7037–7045.
- 18 G. Cotin, B. Heinrich, F. Pertion, C. Kiefer, G. Francius, D. Mertz, B. Freis, B. Pichon, J. Strub, S. Cianferani, N. Ortiz Peña, D. Ihiawakrim, D. Portehault, O. Ersen, A. Khammari, M. Picher, F. Banhart, C. Sanchez and S. Begin-Colin, *Small*, 2022, 2200414.
- 19 J. Park, K. An, Y. Hwang, J.-G. Park, H.-J. Noh, J.-Y. Kim, J.-H. Park, N.-M. Hwang and T. Hyeon, *Nature Mater*, 2004, **3**, 891–895.
- 20 S. Sun and H. Zeng, *J. Am. Chem. Soc.*, 2002, **124**, 8204–8205.
- 21 S. Sun, H. Zeng, D. B. Robinson, S. Raoux, P. M. Rice, S. X. Wang and G. Li, *J. Am. Chem. Soc.*, 2004, **126**, 273–279.
- 22 F. X. Redl, C. T. Black, G. C. Papaefthymiou, R. L. Sandstrom, M. Yin, H. Zeng, C. B. Murray and S. P. O'Brien, *J. Am. Chem. Soc.*, 2004, **126**, 14583–14599.
- 23 J. Park, K. An, Y. Hwang, J.-G. Park, H.-J. Noh, J.-Y. Kim, J.-H. Park, N.-M. Hwang and T. Hyeon, *Nat Mater*, 2004, **3**, 891–895.
- 24 A. Demortière, P. Panissod, B. P. Pichon, G. Pourroy, D. Guillon, B. Donnio and S. Bégin-Colin, *Nanoscale*, 2011, **3**, 225–232.
- 25 E. Wetterskog, C.-W. Tai, J. Grins, L. Bergström and G. Salazar-Alvarez, *ACS Nano*, 2013, **7**, 7132–7144.
- 26 A. Lak, M. Kraken, F. Ludwig, A. Kornowski, D. Eberbeck, S. Sievers, F. J. Litterst, H. Weller and M. Schilling, *Nanoscale*, 2013, **5**, 12286.

- 27 B. P. Pichon, O. Gerber, C. Lefevre, I. Florea, S. Fleutot, W. Baaziz, M. Pauly, M. Ohlmann, C. Ulhaq, O. Ersen, V. Pierron-Bohnes, P. Panissod, M. Drillon and S. Begin-Colin, *Chem. Mater.*, 2011, **23**, 2886–2900.
- 28 H. T. Hai, H. T. Yang, H. Kura, D. Hasegawa, Y. Ogata, M. Takahashi and T. Ogawa, *Journal of Colloid and Interface Science*, 2010, **346**, 37–42.
- 29 X. Sun, N. Frey Huls, A. Sigdel and S. Sun, *Nano Letters*, 2012, **12**, 246–251.
- 30 A. Walter, C. Billotey, A. Garofalo, C. Ulhaq-Bouillet, C. Lefèvre, J. Taleb, S. Laurent, L. Vander Elst, R. N. Muller, L. Lartigue, F. Gazeau, D. Felder-Flesch and S. Begin-Colin, *Chem. Mater.*, 2014, **26**, 5252–5264.
- 31 W. Baaziz, B. P. Pichon, Y. Liu, J.-M. Grenèche, C. Ulhaq-Bouillet, E. Terrier, N. Bergeard, V. Halté, C. Boeglin, F. Choueikani, M. Toumi, T. Mhiri and S. Begin-Colin, *Chemistry of Materials*, 2014, **26**, 5063–5073.
- 32 W. Baaziz, B. P. Pichon, C. Lefevre, C. Ulhaq-Bouillet, J.-M. Greneche, M. Toumi, T. Mhiri and S. Bégin-Colin, *J. Phys. Chem. C*, 2013, **117**, 11436–11443.
- 33 G. Cotin, C. Kiefer, F. Pertont, M. Boero, B. Özdamar, A. Bouzid, G. Ori, C. Massobrio, D. Begin, B. Pichon, D. Mertz and S. Begin-Colin, *ACS Applied Nano Materials*, 2018, **1**, 4306–4316.
- 34 A. N. Shipway, E. Katz and I. Willner, *Chemphyschem*, 2000, **1**, 18–52.
- 35 D. A. J. Herman, S. Cheong-Tilley, A. J. McGrath, B. F. P. McVey, M. Lein and R. D. Tilley, *Nanoscale*, 2015, **7**, 5951–5954.
- 36 W. Baaziz, B. P. Pichon, S. Fleutot, Y. Liu, C. Lefevre, J.-M. Greneche, M. Toumi, T. Mhiri and S. Begin-Colin, *J. Phys. Chem. C*, 2014, **118**, 3795–3810.
- 37 A. Demortière, P. Panissod, B. P. Pichon, G. Pourroy, D. Guillon, B. Donnio and S. Bégin-Colin, *Nanoscale*, 2011, **3**, 225–232.
- 38 G. Cotin, F. Pertont, C. Petit, S. Sall, C. Kiefer, V. Begin, B. Pichon, C. Lefevre, D. Mertz, J.-M. Greneche and S. Begin-Colin, *Chem. Mater.*, 2020, **32**, 9245–9259.
- 39 M. V. Kovalenko, M. I. Bodnarchuk, R. T. Lechner, G. Hesser, F. Schäffler and W. Heiss, *J. Am. Chem. Soc.*, 2007, **129**, 6352–6353.
- 40 U. Jeong, X. Teng, Y. Wang, H. Yang and Y. Xia, *Advanced Materials*, 2007, **19**, 33–60.
- 41 J. van Embden, A. S. R. Chesman and J. J. Jasieniak, *Chem. Mater.*, 2015, **27**, 2246–2285.
- 42 S. G. Kwon and T. Hyeon, *Small*, 2011, **7**, 2685–2702.
- 43 G. Cotin, C. Kiefer, F. Pertont, D. Ihiwakrim, C. Blanco-Andujar, S. Moldovan, C. Lefevre, O. Ersen, B. Pichon, D. Mertz and S. Bégin-Colin, *Nanomaterials*, 2018, **8**, 881.
- 44 L. M. Bronstein, J. E. Atkinson, A. G. Malyutin, F. Kidwai, B. D. Stein, D. G. Morgan, J. M. Perry and J. A. Karty, *Langmuir*, 2011, **27**, 3044–3050.
- 45 G. Salas, C. Casado, F. J. Teran, R. Miranda, C. J. Serna and M. P. Morales, *Journal of Materials Chemistry*, 2012, **22**, 21065–21075.
- 46 P. Guardia, R. Di Corato, L. Lartigue, C. Wilhelm, A. Espinosa, M. Garcia-Hernandez, F. Gazeau, L. Manna and T. Pellegrino, *ACS Nano*, 2012, **6**, 3080–3091.
- 47 P. Guardia, A. Riedinger, S. Nitti, G. Pugliese, S. Marras, A. Genovese, M. E. Materia, C. Lefevre, L. Manna and T. Pellegrino, *J. Mater. Chem. B*, 2014, **2**, 4426–4434.
- 48 G. Cotin, F. Pertont, C. Petit, S. Sall, C. Kiefer, V. Begin, B. Pichon, C. Lefevre, D. Mertz, J.-M. Greneche and S. Begin-Colin, *Chem. Mater.*, 2020, **32**, 9245–9259.
- 49 G. Cotin, C. Blanco-Andujar, F. Pertont, L. Asín, J. M. de la Fuente, W. Reichardt, D. Schaffner, D.-V. Ngyen, D. Mertz, C. Kiefer, F. Meyer, S. Spassov, O. Ersen, M. Chatzidakis, G. A. Botton, C. Hénoumont, S. Laurent, J.-M. Greneche, F. J. Teran, D. Ortega, D. Felder-Flesch and S. Begin-Colin, *Nanoscale*, 2021, **13**, 14552–14571.

- 50 I. Castellanos-Rubio, O. Arriortua, D. Iglesias-Rojas, A. Barón, I. Rodrigo, L. Marcano, J. S. Garitaonandia, I. Orue, M. L. Fdez-Gubieda and M. Insausti, *Chem. Mater.*, 2021, **33**, 8693–8704.
- 51 R. Chen, M. G. Christiansen, A. Sourakov, A. Mohr, Y. Matsumoto, S. Okada, A. Jasanoff and P. Anikeeva, *Nano Lett.*, 2016, **16**, 1345–1351.
- 52 L. Qiao, Z. Fu, J. Li, J. Ghosen, M. Zeng, J. Stebbins, P. N. Prasad and M. T. Swihart, *ACS Nano*, 2017, **11**, 6370–6381.
- 53 L. M. Bronstein, X. Huang, J. Retrum, A. Schmucker, M. Pink, B. D. Stein and B. Dragnea, *Chemistry of Materials*, 2007, **19**, 3624–3632.
- 54 L. M. Bronstein, J. E. Atkinson, A. G. Malyutin, F. Kidwai, B. D. Stein, D. G. Morgan, J. M. Perry and J. A. Karty, *Langmuir*, 2011, **27**, 3044–3050.
- 55 C. J. Meledandri, J. K. Stolarczyk, S. Ghosh and D. F. Brougham, *Langmuir*, 2008, **24**, 14159–14165.
- 56 N. R. Jana, Y. Chen and X. Peng, *Chemistry of Materials*, 2004, **16**, 3931–3935.
- 57 J. M. Vargas and R. D. Zysler, *Nanotechnology*, 2005, **16**, 1474–1476.
- 58 R. Hufschmid, H. Arami, R. M. Ferguson, M. Gonzales, E. Teeman, L. N. Brush, N. D. Browning and K. M. Krishnan, *Nanoscale*, 2015, **7**, 11142–11154.
- 59 L. M. Bronstein, X. Huang, J. Retrum, A. Schmucker, M. Pink, B. D. Stein and B. Dragnea, *Chem. Mater.*, 2007, **19**, 3624–3632.
- 60 K. M. Kirkpatrick, B. H. Zhou, P. C. Bunting and J. D. Rinehart, *Chem. Mater.*, 2022, **34**, 8043–8053.
- 61 T. Balakrishnan, M.-J. Lee, J. Dey and S.-M. Choi, *CrystEngComm*, 2019, **21**, 4063–4071.
- 62 G. Cotin, C. Kiefer, F. Pertion, M. Boero, B. Özdamar, A. Bouzid, G. Ori, C. Massobrio, D. Begin, B. Pichon, D. Mertz and S. Begin-Colin, *ACS Appl. Nano Mater.*, 2018, **1**, 4306–4316.
- 63 T. Belin, N. Guigue-Millot, T. Caillot, D. Aymes and J. C. Niepce, *Journal of Solid State Chemistry*, 2002, **163**, 459–465.
- 64 T. J. Daou, G. Pourroy, S. Bégin-Colin, J. M. Grenèche, C. Ulhaq-Bouillet, P. Legaré, P. Bernhardt, C. Leuvrey and G. Rogez, *Chem. Mater.*, 2006, **18**, 4399–4404.
- 65 J.-P. Jolivet and E. Tronc, *Journal of Colloid and Interface Science*, 1988, **125**, 688–701.
- 66 N. Guigue-Millot, Y. Champion, M. J. Hÿtch, F. Bernard, S. Bégin-Colin and P. Perriat, *The Journal of Physical Chemistry B*, 2001, **105**, 7125–7132.
- 67 J. Santoyo Salazar, L. Perez, O. de Abril, L. Truong Phuoc, D. Ihiwakrim, M. Vazquez, J.-M. Grenèche, S. Begin-Colin and G. Pourroy, *Chem. Mater.*, 2011, **23**, 1379–1386.
- 68 T. J. Daou, G. Pourroy, S. Bégin-Colin, J. M. Grenèche, C. Ulhaq-Bouillet, P. Legaré, P. Bernhardt, C. Leuvrey and G. Rogez, *Chem. Mater.*, 2006, **18**, 4399–4404.
- 69 M. Jeon, M. V. Halbert, Z. R. Stephen and M. Zhang, *Advanced Materials*, 2021, **33**, 1906539.
- 70 E. Wetterskog, C.-W. Tai, J. Grins, L. Bergström and G. Salazar-Alvarez, *ACS Nano*, 2013, **7**, 7132–7144.
- 71 B. P. Pichon, O. Gerber, C. Lefevre, I. Florea, S. Fleutot, W. Baaziz, M. Pauly, M. Ohlmann, C. Ulhaq, O. Ersen, V. Pierron-Bohnes, P. Panissod, M. Drillon and S. Begin-Colin, *Chem. Mater.*, 2011, **23**, 2886–2900.
- 72 H. T. Hai, H. T. Yang, H. Kura, D. Hasegawa, Y. Ogata, M. Takahashi and T. Ogawa, *Journal of Colloid and Interface Science*, 2010, **346**, 37–42.
- 73 C. Hofmann, I. Rusakova, T. Ould-Ely, D. Prieto-Centurión, K. B. Hartman, A. T. Kelly, A. Lüttge and K. H. Whitmire, *Adv. Funct. Mater.*, 2008, **18**, 1661–1667.

- 74 L. M. Bronstein, X. Huang, J. Retrum, A. Schmucker, M. Pink, B. D. Stein and B. Dragnea, *Chem. Mater.*, 2007, **19**, 3624–3632.
- 75 S. G. Kwon, Y. Piao, J. Park, S. Angappane, Y. Jo, N.-M. Hwang, J.-G. Park and T. Hyeon, *J. Am. Chem. Soc.*, 2007, **129**, 12571–12584.
- 76 A. Lak, M. Cassani, B. T. Mai, N. Winckelmans, D. Cabrera, E. Sadrollahi, S. Marras, H. Remmer, S. Fiorito, L. Cremades-Jimeno, F. J. Litterst, F. Ludwig, L. Manna, F. J. Teran, S. Bals and T. Pellegrino, *Nano Lett.*, 2018, 11.
- 77 A. Walter, C. Billotey, A. Garofalo, C. Ulhaq-Bouillet, C. Lefèvre, J. Taleb, S. Laurent, L. Vander Elst, R. N. Muller, L. Lartigue, F. Gazeau, D. Felder-Flesch and S. Begin-Colin, *Chem. Mater.*, 2014, **26**, 5252–5264.
- 78 A. Lak, M. Cassani, B. T. Mai, N. Winckelmans, D. Cabrera, E. Sadrollahi, S. Marras, H. Remmer, S. Fiorito and L. Cremades-Jimeno, *Nano letters*, 2018, **18**, 6856–6866.
- 79 A. Lappas, G. Antonaropoulos, K. Brintakis, M. Vasilakaki, K. N. Trohidou, V. Iannotti, G. Ausanio, A. Kostopoulou, M. Abeykoon and I. K. Robinson, *Physical Review X*, 2019, **9**, 041044.
- 80 P. Guardia, A. Labarta and X. Batlle, *The Journal of Physical Chemistry C*, 2011, **115**, 390–396.
- 81 I. Castellanos-Rubio, I. Rodrigo, R. Munshi, O. Arriortua, J. S. Garitaonandia, A. Martinez-Amesti, F. Plazaola, I. Orue, A. Pralle and M. Insausti, *Nanoscale*, 2019, **11**, 16635–16649.
- 82 R. M. Cornell and U. Schwertmann, *The iron oxides : structure, properties, reactions, occurrences, and uses*, Wiley-VCH, Weinheim :, Second, Completely and Extended Edition., 2003.
- 83 N. T. K. Thanh, Ed., *Clinical applications of magnetic nanoparticles: design to diagnosis manufacturing to medicine*, CRC Press, Taylor & Francis Group, Boca Raton, 2018.
- 84 A. U. Gehring, H. Fischer, M. Louvel, K. Kunze and P. G. Weidler, *Geophysical Journal International*, 2009, **179**, 1361–1371.
- 85 J. Estelrich, E. Escribano, J. Queralt and M. Busquets, *International Journal of Molecular Sciences*, 2015, **16**, 8070–8101.
- 86 N. Lee and T. Hyeon, *Chem. Soc. Rev.*, 2012, **41**, 2575–2589.
- 87 S. Laurent, D. Forge, M. Port, A. Roch, C. Robic, L. Vander Elst and R. N. Muller, *Chemical Reviews*, 2008, **108**, 2064–2110.
- 88 H. B. Na, I. C. Song and T. Hyeon, *Advanced Materials*, 2009, **21**, 2133–2148.
- 89 A. K. Gupta and M. Gupta, *Biomaterials*, 2005, **26**, 3995–4021.
- 90 C. Blanco-Andujar, A. Walter, G. Cotin, C. Bordeianu, D. Mertz, D. Felder-Flesch and S. Begin-Colin, *Nanomedicine (London, England)*, 2016, **11**, 1889–1910.
- 91 D. Kim, J. Kim, Y. I. Park, N. Lee and T. Hyeon, *ACS Cent. Sci.*, 2018, **4**, 324–336.
- 92 W. A. Gibby, *Neurosurgery Clinics of North America*, 2005, **16**, 1–64.
- 93 J. P. Ridgway, *Journal of Cardiovascular Magnetic Resonance*, 2010, **12**, 71.
- 94 Z. Jászberényi, A. Sour, É. Tóth, M. Benmelouka and A. Merbach, *Dalton Transactions*, 2005, 2713.
- 95 H. Duan, M. Kuang, X. Wang, Y. A. Wang, H. Mao and S. Nie, *J. Phys. Chem. C*, 2008, **112**, 8127–8131.
- 96 P. A. Rinck, *Magnetic Resonance in Medicine*.
- 97 Y.-D. Xiao, R. Paudel, J. Liu, C. Ma, Z.-S. Zhang and S.-K. Zhou, *International Journal of Molecular Medicine*, 2016, **38**, 1319–1326.
- 98 J. W. M. Bulte and D. L. Kraitman, *NMR in Biomedicine*, 2004, **17**, 484–499.

- 99 Barbara Freis, G. Cotin, F. Pertion, D. Mertz, S. Boutry, S. Laurent and S. Begin-Colin, *Magnetic Nanoparticles in Human Health and Medicine*, 2021, 380–429.
- 100 L. Li, W. Jiang, K. Luo, H. Song, F. Lan, Y. Wu and Z. Gu, *Theranostics*, 2013, **3**, 595–615.
- 101 J. W. M. Bulte, *American Journal of Roentgenology*, 2009, **193**, 314–325.
- 102 M. Kresse, S. Wagner, D. Pfefferer, R. Lawaczek, V. Elste and W. Semmler, *Magn. Reson. Med.*, 1998, **40**, 236–242.
- 103 C. L. Dennis, K. L. Krycka, J. A. Borchers, R. D. Desautels, J. van Lierop, N. F. Huls, A. J. Jackson, C. Gruettner and R. Ivkov, *Advanced Functional Materials*, 2015, **25**, 4300–4311.
- 104 C. Blanco-Andujar, D. Ortega, P. Southern, Q. A. Pankhurst and N. T. K. Thanh, *Nanoscale*, 2015, **7**, 1768–1775.
- 105 B. Luigjes, S. M. C. Woudenberg, R. de Groot, J. D. Meeldijk, H. M. Torres Galvis, K. P. de Jong, A. P. Philipse and B. H. Erné, *J. Phys. Chem. C*, 2011, **115**, 14598–14605.
- 106 GLOBOCAN 2020 cancer incidence, <https://gco.iarc.fr/today/>, (accessed April 14, 2023).
- 107 A. K. Abbas and A. H. Lichtman, *Basic immunology : functions and disorders of the immune system - NLM Catalog - NCBI*, United State, 3rd edn., 2015.
- 108 L. Q. Chow, C. Chen and D. Raben, *Current Cancer Therapy Reviews*, 2007, **3**, 255–266.
- 109 B. P. Pollack, B. Sapkota and T. V. Cartee, *Clin Cancer Res*, 2011, **17**, 4400–4413.
- 110 K. C. Valkenburg, A. E. de Groot and K. J. Pienta, *Nat Rev Clin Oncol*, 2018, **15**, 366–381.
- 111 K. Thankappan, S. Iyer and J. Menon, *Dysphagia Management in Head and Neck Cancers A Manual and Atlas: A Manual and Atlas*, 2018.
- 112 X. Gao, S. Wang, Z. Tian, Y. Wu and W. Liu, *Transl Cancer Res*, 2021, **10**, 251–260.
- 113 D. Pulte and H. Brenner, *Oncologist*, 2010, **15**, 994–1001.
- 114 S. Indoria, V. Singh and M.-F. Hsieh, *International Journal of Pharmaceutics*, 2020, **582**, 119314.
- 115 A.-G. Niculescu and A. M. Grumezescu, *International Journal of Molecular Sciences*, 2022, **23**, 5253.
- 116 A. Aghebati-Maleki, S. Dolati, M. Ahmadi, A. Baghbanzadeh, M. Asadi, A. Fotouhi, M. Yousefi and L. Aghebati-Maleki, *Journal of Cellular Physiology*, 2020, **235**, 1962–1972.
- 117 M. J. Mitchell, M. M. Billingsley, R. M. Haley, M. E. Wechsler, N. A. Peppas and R. Langer, *Nat Rev Drug Discov*, 2021, **20**, 101–124.
- 118 M. F. Attia, N. Anton, J. Wallyn, Z. Omran and T. F. Vandamme, *J Pharm Pharmacol*, 2019, **71**, 1185–1198.
- 119 A. Ruiz, G. Salas, M. Calero, Y. Hernández, A. Villanueva, F. Herranz, S. Veintemillas-Verdaguer, E. Martínez, D. F. Barber and M. P. Morales, *Acta Biomaterialia*, 2013, **9**, 6421–6430.
- 120 N. Hoshyar, S. Gray, H. Han and G. Bao, *Nanomedicine (Lond)*, 2016, **11**, 673–692.
- 121 I. Hilger, *International Journal of Hyperthermia*, 2013, **29**, 828–834.
- 122 X. Liu, Y. Zhang, Y. Wang, W. Zhu, G. Li, X. Ma, Y. Zhang, S. Chen, S. Tiwari and K. Shi, *Theranostics*, 2020, **10**, 3793.
- 123 D. Chang, M. Lim, J. A. Goos, R. Qiao, Y. Y. Ng, F. M. Mansfeld, M. Jackson, T. P. Davis and M. Kavallaris, *Frontiers in pharmacology*, 2018, **9**, 831.
- 124 O. S. Nielsen, M. Horsman and J. Overgaard, *European Journal of Cancer*, 2001, **37**, 1587–1589.
- 125 A. Villanueva, P. de la Presa, J. M. Alonso, T. Rueda, A. Martínez, P. Crespo, M. P. Morales, M. A. Gonzalez-Fernandez, J. Valdés and G. Rivero, *J. Phys. Chem. C*, 2010, **114**, 1976–1981.

- 126G. F. Goya, L. Asín and M. R. Ibarra, *International Journal of Hyperthermia*, 2013, **29**, 810–818.
- 127J. R. Lepock, *International Journal of Hyperthermia*, 2005, **21**, 681–687.
- 128J. R. Lepock, *Methods*, 2005, **35**, 117–125.
- 129A. J. Peer, M. J. Grimm, E. R. Zynda and E. A. Repasky, *Immunol Res*, 2010, **46**, 137–154.
- 130P. de Andrade Mello, S. Bian, L. E. B. Savio, H. Zhang, J. Zhang, W. Junger, M. R. Wink, G. Lenz, A. Buffon, Y. Wu and S. C. Robson, *Oncotarget*, 2017, **8**, 67254–67268.
- 131K. L. Eales, K. E. R. Hollinshead and D. A. Tennant, *Oncogenesis*, 2016, **5**, e190.
- 132D. Ortega and Q. A. Pankhurst, in *Nanoscience*, ed. P. O'Brien, Royal Society of Chemistry, Cambridge, 2012, vol. 1, pp. 60–88.
- 133R. Hergt and S. Dutz, *Journal of Magnetism and Magnetic Materials*, 2007, **311**, 187–192.
- 134M. Domenech, I. Marrero-Berrios, M. Torres-Lugo and C. Rinaldi, *ACS Nano*, 2013, **7**, 5091–5101.
- 135M. Creixell, A. C. Bohórquez, M. Torres-Lugo and C. Rinaldi, *ACS Nano*, 2011, **5**, 7124–7129.
- 136H. F. Krug and P. Wick, *Angew Chem Int Ed Engl*, 2011, **50**, 1260–1278.
- 137A. Elengoe and S. Hamdan, *International Journal of Advancement in Life Sciences Research*, 2018, 22–27.
- 138I. Takahashi, Y. Emi, S. Hasuda, Y. Kakeji, Y. Maehara and K. Sugimachi, *Surgery*, 2002, **131**, S78–S84.
- 139Z. Behrouzkia, Z. Joveini, B. Keshavarzi, N. Eyvazzadeh and R. Z. Aghdam, *Oman Med J*, 2016, **31**, 89–97.
- 140V. Ejigah, O. Owoseni, P. Bataille-Backer, O. D. Ogundipe, F. A. Fisusi and S. K. Adesina, *Polymers*, 2022, **14**, 2601.
- 141Y. Matsumura and H. Maeda, *Cancer Res*, 1986, **46**, 6387–6392.
- 142E. Alphandéry, S. Faure, L. Raison, E. Duguet, P. A. Howse and D. A. Bazylnski, *J. Phys. Chem. C*, 2011, **115**, 18–22.
- 143M. K. Yu, J. Park and S. Jon, *Theranostics*, 2012, **2**, 3–44.
- 144S. Wilhelm, A. J. Tavares, Q. Dai, S. Ohta, J. Audet, H. F. Dvorak and W. C. W. Chan, *Nat Rev Mater*, 2016, **1**, 1–12.
- 145R. Bazak, M. Hour, S. El Achy, S. Kamel and T. Refaat, *J Cancer Res Clin Oncol*, 2015, **141**, 769–784.
- 146A. L. C. de S. L. Oliveira, T. Schomann, L.-F. de Geus-Oei, E. Kapiteijn, L. J. Cruz and R. F. de Araújo Junior, *Pharmaceutics*, 2021, **13**, 1321.
- 147E. Y. Makhani, A. Zhang and J. B. Haun, *Nano Convergence*, 2021, **8**, 38.
- 148V. Torchilin, *Advanced Drug Delivery Reviews*, 2011, **63**, 131–135.
- 149S. Chono, T. Tanino, T. Seki and K. Morimoto, *Journal of Pharmacy and Pharmacology*, 2007, **59**, 75–80.
- 150H. Maeda, T. Sawa and T. Konno, *Journal of Controlled Release*, 2001, **74**, 47–61.
- 151H. Kobayashi, R. Watanabe and P. L. Choyke, *Theranostics*, 2013, **4**, 81–89.
- 152M. O. Oyewumi, R. A. Yokel, M. Jay, T. Coakley and R. J. Mumper, *Journal of Controlled Release*, 2004, **95**, 613–626.
- 153A. Angelopoulou, A. Kolokithas-Ntoukas, C. Fytas and K. Avgoustakis, *ACS Omega*, 2019, **4**, 22214–22227.
- 154M. Truffi, M. Colombo, L. Sorrentino, L. Pandolfi, S. Mazzucchelli, F. Pappalardo, C. Pacini, R. Allevi, A. Bonizzi, F. Corsi and D. Prosperi, *Sci Rep*, 2018, **8**, 6563.
- 155R. Bazak, M. Hour, S. El Achy, S. Kamel and T. Refaat, *J Cancer Res Clin Oncol*, 2015, **141**, 769–784.

- 156J. Yoo, C. Park, G. Yi, D. Lee and H. Koo, *Cancers (Basel)*, 2019, **11**, E640.
- 157G. T. Tietjen, L. G. Bracaglia, W. M. Saltzman and J. S. Pober, *Trends Mol Med*, 2018, **24**, 598–606.
- 158C. NDong, J. A. Tate, W. C. Kett, J. Batra, E. Demidenko, L. D. Lewis, P. J. Hoopes, T. U. Gerngross and K. E. Griswold, *PLoS One*, 2015, **10**, e0115636.
- 159S. Palanisamy and Y.-M. Wang, *Dalton Trans.*, 2019, **48**, 9490–9515.
- 160V. Mittelheisser, P. Coliat, E. Moeglin, L. Goepp, J. G. Goetz, L. J. Charbonnière, X. Pivot and A. Detappe, *Advanced Materials*, 2022, **34**, 2110305.
- 161M. K. Yu, J. Park and S. Jon, *Theranostics*, 2012, **2**, 3–44.
- 162E. Alphandéry, *Nanotoxicology*, 2019, **13**, 573–596.
- 163A. Ahmad, F. Khan, R. K. Mishra and R. Khan, *J. Med. Chem.*, 2019, **62**, 10475–10496.
- 164J. D. Byrne, T. Betancourt and L. Brannon-Peppas, *Advanced Drug Delivery Reviews*, 2008, **60**, 1615–1626.
- 165T. M. Allen, *Nat Rev Cancer*, 2002, **2**, 750–763.
- 166G. T. Hermanson, *Bioconjugate Techniques*, Academic Press, 2013.
- 167T. Iwasawa, P. Wash, C. Gibson and J. Rebek, *Tetrahedron*, 2007, **63**, 6506–6511.
- 168D. P. Nair, M. Podgórski, S. Chatani, T. Gong, W. Xi, C. R. Fenoli and C. N. Bowman, *Chem. Mater.*, 2014, **26**, 724–744.
- 169N. Guldris, J. Gallo, L. García-Hevia, J. Rivas, M. Bañobre-López and L. M. Salonen, *Chemistry – A European Journal*, 2018, **24**, 8624–8631.
- 170J. Pellico, P. J. Gawne and R. T. M. de Rosales, *Chemical Society Reviews*, 2021, **50**, 3355–3423.
- 171J. Nam, N. Won, J. Bang, H. Jin, J. Park, S. Jung, S. Jung, Y. Park and S. Kim, *Advanced Drug Delivery Reviews*, 2013, **65**, 622–648.
- 172B. Freis, M. D. L. Á. Ramírez, S. Furgiuele, F. Journe, C. Cheignon, L. J. Charbonnière, C. Henoumont, C. Kiefer, D. Mertz, C. Affolter-Zbaraszczuk, F. Meyer, S. Saussez, S. Laurent, M. Tasso and S. Bégin-Colin, *International Journal of Pharmaceutics*, 2023, **635**, 122654.
- 173G. Rimkus, S. Bremer-Streck, C. Grüttner, W. A. Kaiser and I. Hilger, *Contrast Media Mol Imaging*, 2011, **6**, 119–125.
- 174P. Foroozandeh and A. A. Aziz, *Nanoscale Res Lett*, 2018, **13**, 339.
- 175B. Svitkova, V. Zavisova, V. Nemethova, M. Koneracka, M. Kretova, F. Razga, M. Ursinyova and A. Gabelova, *Beilstein J. Nanotechnol.*, 2021, **12**, 270–281.
- 176H. Hossein-Nejad-Ariani, E. Althagafi and K. Kaur, *Sci Rep*, 2019, **9**, 2723.
- 177J. Estelrich, E. Escribano, J. Queralt and M. A. Busquets, *International journal of molecular sciences*, 2015, **16**, 8070–8101.
- 178M. W. Freeman, A. Arrott and J. H. L. Watson, *Journal of Applied Physics*, 1960, **31**, S404–S405.
- 179Y. Shen, X. Liu, Z. Huang, N. Pei, J. Xu, Z. Li, Y. Wang, J. Qian and J. Ge, *Cell Transplant*, 2015, **24**, 1981–1997.
- 180S. Zhao, X. Yu, Y. Qian, W. Chen and J. Shen, *Theranostics*, 2020, **10**, 6278–6309.
- 181R. Baskar, K. A. Lee, R. Yeo and K.-W. Yeoh, *Int J Med Sci*, 2012, **9**, 193–199.
- 182Y. Liu, P. Zhang, F. Li, X. Jin, J. Li, W. Chen and Q. Li, *Theranostics*, 2018, **8**, 1824–1849.
- 183K. Haume, S. Rosa, S. Grellet, M. A. Śmiałek, K. T. Butterworth, A. V. Solov'yov, K. M. Prise, J. Golding and N. J. Mason, *Cancer Nanotechnology*, 2016, **7**, 8.
- 184J. F. Hainfeld, D. N. Slatkin and H. M. Smilowitz, *Phys Med Biol*, 2004, **49**, N309–315.
- 185S. Li, S. Bouchy, S. Penninckx, R. Marega, O. Fichera, B. Gallez, O. Feron, P. Martinive, A.-C. Heuskin, C. Michiels and S. Lucas, *Nanomedicine (Lond)*, 2019, **14**, 317–333.

- 186N. G. Shetake, A. Kumar and B. N. Pandey, *Biochimica et Biophysica Acta (BBA) - General Subjects*, 2019, **1863**, 857–869.
- 187R. Ahmad, G. Schettino, G. Royle, M. Barry, Q. A. Pankhurst, O. Tillement, B. Russell and K. Ricketts, *Part Part Syst Charact*, 2020, **37**, 1900411.
- 188I. Ternad, S. Penninckx, V. Lecomte, T. Vangijzegem, L. Conrard, S. Lucas, A.-C. Heuskin, C. Michiels, R. N. Muller, D. Stanicki and S. Laurent, *Nanomaterials*, 2023, **13**, 201.
- 189V. Schirmmacher, *International Journal of Oncology*, 2019, **54**, 407–419.
- 190A. Mohammad, *Open Access Journal of Toxicology*, , DOI:10.19080/OAJT.2018.02.555600.
- 191D. Huang, H. Duan, H. Huang, X. Tong, Y. Han, G. Ru, L. Qu, C. Shou and Z. Zhao, *Sci Rep*, 2016, **6**, 20502.
- 192K. B. Challagundla, P. M. Wise, P. Neviani, H. Chava, M. Murtadha, T. Xu, R. Kennedy, C. Ivan, X. Zhang, I. Vannini, F. Fanini, D. Amadori, G. A. Calin, M. Hadjidaniel, H. Shimada, A. Jong, R. C. Seeger, S. Asgharzadeh, A. Goldkorn and M. Fabbri, *JNCI: Journal of the National Cancer Institute*, 2015, **107**, djv135.
- 193X. Wang, H. Zhang and X. Chen, *Cancer Drug Resistance*, 2019, **2**, 141–160.
- 194Y. Huang, K. Mao, B. Zhang and Y. Zhao, *Materials Science and Engineering: C*, 2017, **70**, 763–771.
- 195P. Eslami, M. Albino, F. Scavone, F. Chiellini, A. Morelli, G. Baldi, L. Cappiello, S. Doumet, G. Lorenzi, C. Ravagli, A. Caneschi, A. Laurenzana and C. Sangregorio, *Nanomaterials (Basel)*, 2022, **12**, 303.
- 196M. H. El-Dakdouki, D. C. Zhu, K. El-Boubbou, M. Kamat, J. Chen, W. Li and X. Huang, *Biomacromolecules*, 2012, **13**, 1144–1151.
- 197M. H. El-Dakdouki, J. Xia, D. C. Zhu, H. Kavunja, J. Grieshaber, S. O'Reilly, J. J. McCormick and X. Huang, *ACS Appl. Mater. Interfaces*, 2014, **6**, 697–705.
- 198S.-W. Lee, Y.-M. Kim, C. H. Cho, Y. T. Kim, S. M. Kim, S. Y. Hur, J.-H. Kim, B.-G. Kim, S.-C. Kim, H.-S. Ryu and S. B. Kang, *Cancer Res Treat*, 2018, **50**, 195–203.
- 199E. Guisasola, L. Asín, L. Beola, J. M. de la Fuente, A. Baeza and M. Vallet-Regí, *ACS Appl. Mater. Interfaces*, 2018, **10**, 12518–12525.
- 200Y. Fang, Y. He, C. Wu, M. Zhang, Z. Gu, J. Zhang, E. Liu, Q. Xu, A. M. Asrorov and Y. Huang, *Theranostics*, 2021, **11**, 6860–6872.
- 201T. Vangijzegem, V. Lecomte, I. Ternad, L. Van Leuven, R. N. Muller, D. Stanicki and S. Laurent, *Pharmaceutics*, 2023, **15**, 236.
- 202B. Li and L. Lin, *Light Sci Appl*, 2022, **11**, 85.
- 203T.-J. Yu, P.-H. Li, T.-W. Tseng and Y.-C. Chen, *Nanomedicine*, 2011, **6**, 1353–1363.
- 204H. Chen, J. Burnett, F. Zhang, J. Zhang, H. Paholak and D. Sun, *J. Mater. Chem. B*, 2014, **2**, 757–765.
- 205M.-Y. Liao, P.-S. Lai, H.-P. Yu, H.-P. Lin and C.-C. Huang, *Chem. Commun.*, 2012, **48**, 5319.
- 206S. Shen, F. Kong, X. Guo, L. Wu, H. Shen, M. Xie, X. Wang, Y. Jin and Y. Ge, *Nanoscale*, 2013, **5**, 8056.
- 207Z. Zhou, Y. Sun, J. Shen, J. Wei, C. Yu, B. Kong, W. Liu, H. Yang, S. Yang and W. Wang, *Biomaterials*, 2014, **35**, 7470–7478.
- 208E. A. Hussein, M. M. Zagho, B. R. Rizeq, N. N. Younes, G. Pintus, K. A. Mahmoud, G. K. Nasrallah and A. A. Elzatahry, *International Journal of Nanomedicine*, 2019, **14**, 4529–4539.
- 209A. Pinto and M. Pocard, *Pleura and Peritoneum*, , DOI:10.1515/pp-2018-0124.
- 210L. Wu, L. Chen, F. Liu, X. Qi, Y. Ge and S. Shen, *Colloids and Surfaces B: Biointerfaces*, 2017, **152**, 440–448.

- 211 X. Sun, B. Liu, X. Chen, H. Lin, Y. Peng, Y. Li, H. Zheng, Y. Xu, X. Ou, S. Yan, Z. Wu, S. Deng, L. Zhang and P. Zhao, *J Mater Sci: Mater Med*, 2019, **30**, 76.
- 212 C.-C. Wu, Y.-C. Yang, Y.-T. Hsu, T.-C. Wu, C.-F. Hung, J.-T. Huang and C.-L. Chang, *Oncotarget*, 2015, **6**, 26861–26875.

Acronyms

AMF: Alternating magnetic field	PDT: Photodynamic therapy
BSA: Bovine serum albumin	PTT: Photothermal therapy
CA: Contrast agent	RNA: Ribonucleic acid
DBE: Dibenzyl ether	ROS: Reactive oxygen species
D _h : Hydrodynamic diameter	RT: Radiation therapy
DNA: Deoxyribonucleic acid	SAR: Specific absorption rate
Dox.: Doxorubicin	TAM: Tumor-associated macrophage
EGF: Epidermal growth factor	TD: Thermal decomposition
EGFR: Epidermal growth factor receptor	TGA: Thermogravimetric analysis
EPR: Enhanced permeability and retention	TL: Targeting ligand
Fabs: Fragment antigen-binding	TME: Tumoral micro-environment
FDA: Food and drug administration	USPIO: Ultrasmall particle of iron oxide
FID: Free induction decay	WHO: World health organization
FTIR: Fourier transform infrared	XRT: X-rays radiotherapy
GLOBOCAN: Global cancer observatory	
GNP: Gold nanoparticle	
HER: Human epidermal growth factor	
HNC: Head and neck cancers	
IONP: Iron oxide nanoparticle	
IS: Immune system	
i.v.: intravenous	
MH: Magnetic hyperthermia	
MPS: Mononuclear phagocyte system	
MRI: Magnetic resonance imaging	
NK: Natural killer	
NIR: Near-infrared	
NP: Nanoparticle	
OA: Oleic acid	
PEG: Poly-ethylene-glycol	